

Origin of Selectivity in the Antibody 20F10-Catalyzed Yang Cyclization

Sigal Saphier,[†] Yunfeng Hu,[‡] Subhash C. Sinha,[§] K. N. Houk,^{*,†} and Ehud Keinan^{*,†,§}

Contribution from the Department of Chemistry and Institute of Catalysis Science and Technology, Technion—Israel Institute of Technology Technion City, Haifa 32000 Israel, Department of Chemistry and Biochemistry, University of California, Los Angeles, 607 Charles E. Young Drive East, Los Angeles, California 90095-1569, and Department of Molecular Biology and the Skaggs Institute for Chemical Biology, The Scripps Research Institute, 10550 North Torrey Pines Road, La Jolla, California 92037

Received July 29, 2004; E-mail: houk@chem.ucla.edu; keinan@scripps.edu

Abstract: The first antibody-catalyzed Yang (Norrish type II) cyclization has been achieved with antibodies that were elicited against *cis*- and *trans*-2,3-diaryloxetanes. The photocyclization of 1,4-diarylbutan-1-one produced a single stereoisomer of *cis*-1,2-diarylcyclobutanol with very high enantioselectivity. The background photochemical reaction in the absence of the antibody yielded only fragmentation products. The antibody 20F10-catalyzed reaction was studied in detail, exploring its selectivity, substituent effects, substrate and hapten binding, kinetic parameters and irradiation wavelength dependence. Quantum mechanical calculations suggest that the activation enthalpy of fragmentation pathway is favored by 7.9 kcal/mol over cyclization pathway. Hapten, substrate, and transition state docking studies on a homology based modeled antibody binding site indicate that the *trans* hapten, substrate and the cyclization transition state have similar binding modes. By contrast, the fragmentation transition state is bound in a different way, not easily accessible within the lifetime of the bound substrate excited state. Several side chain residues were identified that can act as local sensitizers to enhance the cyclization process.

Introduction

Although life on earth depends on light-induced chemistry, such as photosynthesis, vision, circadian rhythms, plant flowering, seed germination, phototropism, and photomorphogenesis, when searching for a single protein that exploits light to catalyze a specific chemical reaction one finds that only three enzymes that catalyze a specific photoreaction have been reported.¹ These include protochlorophyllide reductase² and two enzymes that catalyze fragmentation of thymine dimers as part of the DNA repair mechanism: DNA photolyase³ and [6–4]-photoproduct lyase.⁴ The very limited diversity of enzymes that catalyze photochemical reactions suggests that evolution has selected against photoenzymes, particularly in multicellular organisms, and yet their particular existence encourages the development of new photoenzymes.

Catalysis of photochemical reactions offers an opportunity to study the conformational effects conferred by those catalysts on the reaction pathway. Biocatalysis represents an attractive strategy to restrain mechanistic manifolds and channel a reactive intermediate into a single product.⁵ Since a photochemical reaction proceeds through a light induced, highly activated intermediate, stabilization of transition state in the classical sense of lowering the activation energy barrier is irrelevant. Other concepts of enzyme catalysis such as entropic trap and restriction of the conformational space or “negative catalysis” are more appropriate in the design of new photocatalytic antibodies.⁶ Understanding the origin of catalysis and mechanism of action in the very few known naturally occurring photocatalysts could help in the design of new catalysts.

While very few antibodies that catalyze photochemical reactions have been reported to date, there are strong indications that photocatalytic antibodies can become attractive synthetic tools and mechanistic probes. The three reported attempts to catalyze photoreactions with antibodies include dimerization of methyl *p*-nitrocinnamate,⁷ cleavage of thymine and uracil

[†] Department of Chemistry and Institute of Catalysis Science and Technology, Technion—Israel Institute of Technology Technion City.

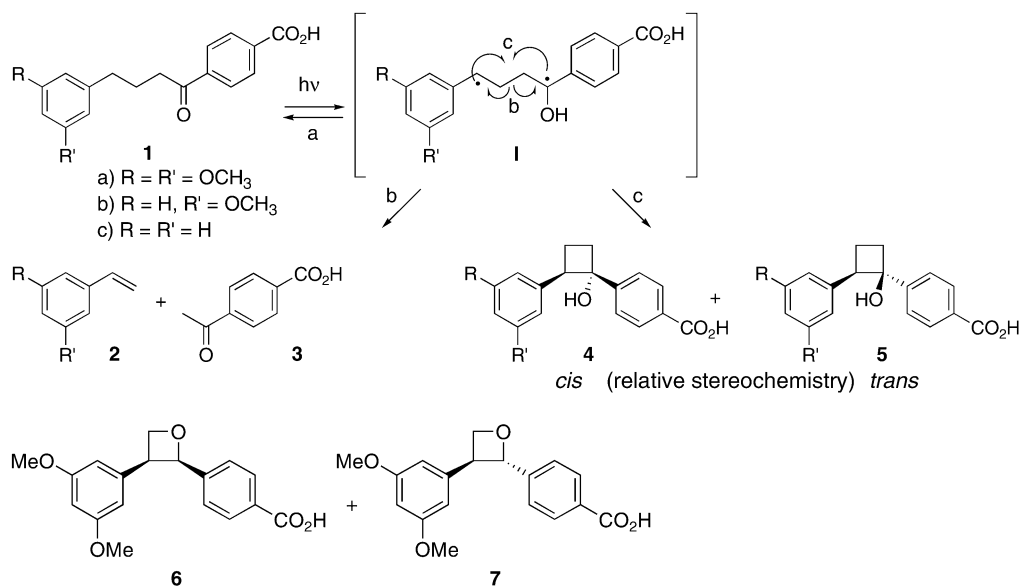
[‡] Department of Chemistry and Biochemistry, University of California, Los Angeles.

[§] Department of Molecular Biology and the Skaggs Institute for Chemical Biology, The Scripps Research Institute.

- (1) (a) Kim, S. T.; Li, Y. F.; Sancar, A. *Proc. Natl. Acad. Sci. U.S.A.* **1992**, *89*, 900–904. (b) Tai, L. A.; Hwang, K. C. *Angew. Chem., Int. Ed.* **2000**, *39*, 3886–3888. (c) Sancar, A. *Chem. Rev.* **2003**, *103*, 2203–2237.
- (2) Begley, T. P. *Acc. Chem. Res.* **1994**, *27*, 394–401.
- (3) Eker, A. P. M.; Hessels, J. K. C.; Dekker, R. H. *Photochem. Photobiol.* **1986**, *44*, 197.
- (4) Todo, T.; Takemori, H.; Ryo, H.; Ihara, M.; Marsunaga, T.; Nikaido, O.; Sato, K.; Nomura, T. *Nature* **1993**, *361*, 371–374.

- (5) (a) Retez, J. *Angew. Chem., Int. Ed. Engl.* **1990**, *29*, 355. (b) Walsh, C. *Enzymatic Reaction Mechanisms*, W. H. Freeman and Company: New York, 1979.
- (6) Saphier, S.; Piran, R.; Keinan, E. In *Catalytic Antibodies*; Keinan, E., Ed.; Wiley-VCH: New York, 2004; Chapter 13: Photoenzymes and photoabzymes; pp 351–368.
- (7) Balan, A.; Docto, B. P.; Green, B. S.; Torton, M.; Ziffer, H. *J. Chem. Soc. Chem. Commun.* **1988**, 106–108.

Scheme 1



cyclobutane dimers⁸ similar to the natural DNA photolyase, and intramolecular hydrogen transfer reaction in an α -ketoamide.⁹

The Norrish type II photochemical reaction involves abstraction of a γ -hydrogen by an excited carbonyl group (e.g., **1**, Scheme 1) to produce a 1,4-diradical intermediate, **I**.¹⁰ The latter can undergo three alternative reactions: (a) reverse hydrogen transfer to regenerate the ground state of **1**; (b) C–C bond cleavage to form an alkene, **2**, and an enol, which can tautomerize to the carbonyl compound, **3**; and (c) radical recombination (Yang cyclization¹¹) to produce cyclobutanols, **4** and **5**. Usually, (b) is the most common route while (c) represents a minor side-reaction. Intense mechanistic studies over the past three decades have made the Norrish type II reaction one of the most well understood photochemical reactions.¹⁰

The most successful approach to limit the photoproducts variability has been based on solid-state reactions, where the crystal packing forces severely restrict the range of available conformations.¹² Attempts to control the reaction by restricting the conformational flexibility of reactants and intermediates by other organized media,¹³ including liquid-crystals,¹⁴ silica gel surfaces,¹⁵ zeolites,¹⁶ inclusion complexes,¹⁷ micelles¹⁸ and

polymer matrixes,¹⁹ have enjoyed only limited success because these environments are not tailor-made for a specific reaction. Thus, for synthetic purposes, these approaches are limited only to cases where the preferred conformation of the reactant is photochemically productive.

Taking a lesson from Scheffer's reports on the successful photocyclization of ketones in the solid state,¹² we envisioned that antibodies elicited against the *cis*- and *trans*-oxetanes, **6** and **7** would restrict the conformational flexibility of **1**, while stabilizing its productive conformation for photochemical cyclization. In our preliminary report, we have shown that indeed, anti-**6** and anti-**7** antibodies selectively catalyzed the formation of a cyclobutanol product in the Norrish type II reaction.²⁰ Furthermore, we have shown that the resultant photoproduct is obtained as a single stereoisomer, with very high enantioselectivity.

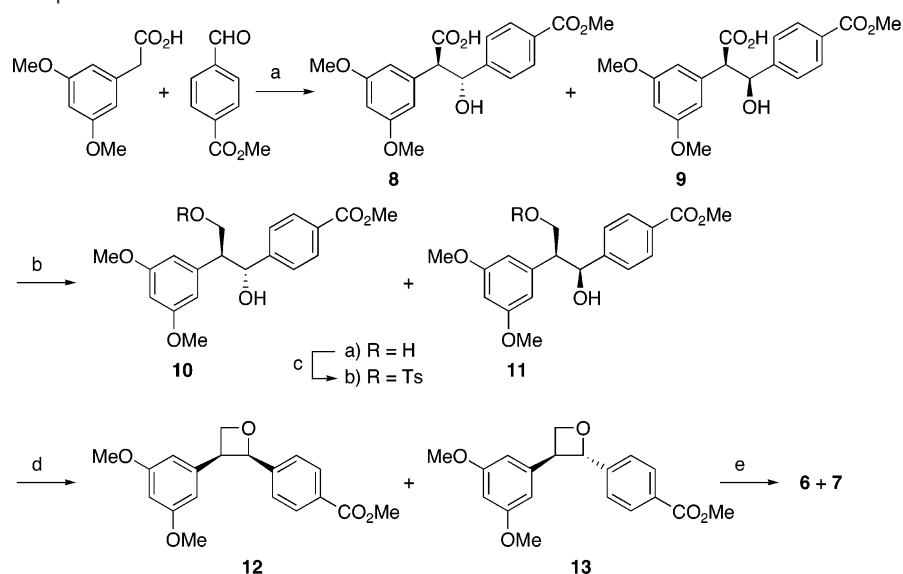
In addition to providing details about the catalysis of the Yang cyclization by antibody 20F10, we report here on the amino acid sequence of this antibody and on the homology modeling with docking experiments of haptens, substrates and transition states. We show that both pseudo-*cis* and pseudo-*trans* substrates bind in the antibody active site, but the transition state for cyclization binds more tightly than the transition state for fragmentation.

Results and Discussion

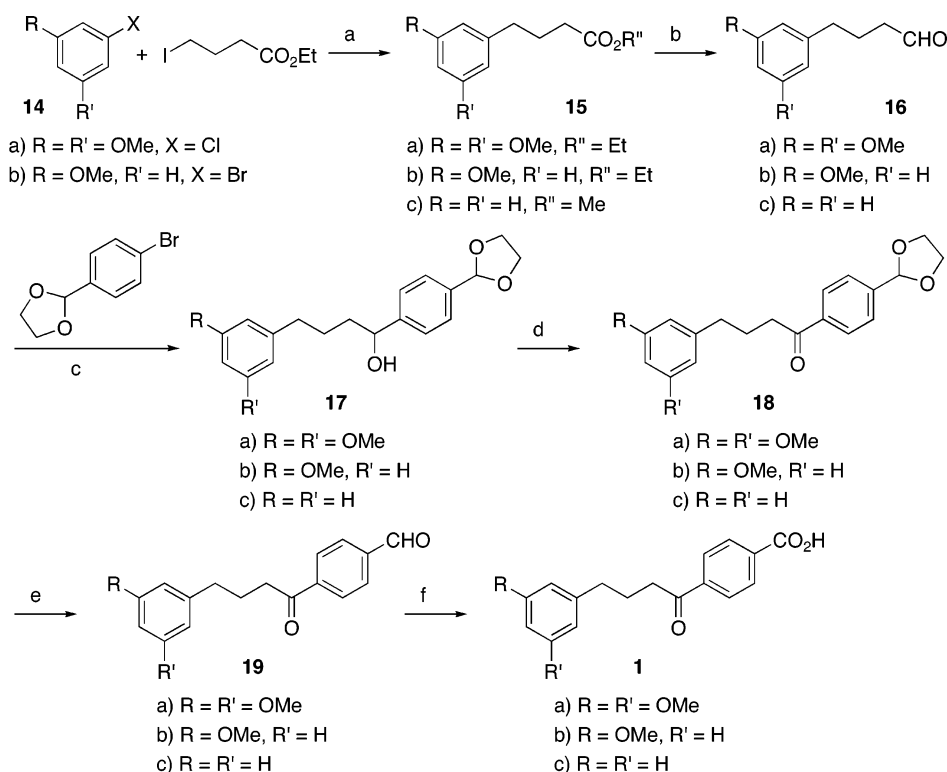
Synthesis of Haptens, Substrates, and Products. Haptens **6** and **7** were synthesized in 5 steps starting with addition of the lithium enolate of 3,5-dimethoxyphenyl acetic acid to methyl-4-formylbenzoate to produce the isomeric hydroxyacids **8** and **9** (Scheme 2). The carboxylic acid was reduced by borane-dimethyl sulfide complex to afford diols **10a** and **11a**. The primary alcohol in both was converted to the corresponding tosylates **10b** and **11b** using *p*-toluenesulfonyl chloride in

- (8) (a) Cochran, A. G.; Sugawara, R.; Schultz, P. G. *J. Am. Chem. Soc.* **1998**, *110*, 7888–7890. (b) Jacobsen, J. R.; Cochran, A. G.; Stephens, J. C.; King, D. S.; Schultz, P. G. *J. Am. Chem. Soc.* **1995**, *117*, 5453–5461.
 (9) Taylor, M. J.; Hoffman, T. Z.; Yli-Kauhaluoma, J. T.; Lerner, R. A.; Janda, K. D. *J. Am. Chem. Soc.* **1998**, *120*, 12783–12790.
 (10) Wagner, P. J. In *CRC Handbook of Organic Photochemistry and Photobiology*; CRC Press: New York, 1995; 449.
 (11) Yang, N. C.; Yang, D. H. *J. Am. Chem. Soc.* **1958**, *80*, 2913–2914.
 (12) (a) Leibovitch, M.; Olovsson, G.; Scheffer, J. R.; Trotter, J. *J. Am. Chem. Soc.* **1998**, *120*, 12755–12769, and references therein. (b) Scheffer, J. R.; Garcia-Garibay, M.; Nalamasu, O. In *Organic Photochemistry*; Padwa, A., Ed.; Marcel Dekker: 1987; 8, Chapter 4, 249–347.
 (13) (a) Inoue, Y. *Chem. Rev.* **1992**, *92*, 741–770. (b) Vishnumurthy, K.; Cheung, E.; Scheffer, J. R.; Scott, C. *Org. Lett.* **2002**, *4*, 1071–1074.
 (14) (a) Furman, I.; Weiss, R. G. *J. Am. Chem. Soc.* **1992**, *114*, 1381–1388. (b) Furman, I.; Catchings, R. M.; Weiss, R. G. *J. Am. Chem. Soc.* **1992**, *114*, 6023–6030.
 (15) Turro, N. J. *Tetrahedron* **1987**, *43*, 1589–1616.
 (16) (a) Turro, N. J.; Wan, P. *Tett. Lett.* **1984**, *25*, 3655–3658. (b) Ramamurthy, V.; Corbin, D. R.; Eaton, D. F. *J. Chem. Soc., Chem. Commun.* **1989**, 1213–1215.
 (17) (a) Casal, H. L.; de Mayo, P.; Miranda, J. F.; Scaiano, J. C. *J. Am. Chem. Soc.* **1983**, *105*, 5155–5156. (b) Goldberg, I. *Top. Curr. Chem.* **1988**, *149*, 1. (c) Vincens, J. *Mol. Cryst. Liq. Cryst.* **1990**, *187*, 115. (d) Kaftory, M.; Toda, F.; Tanaka, K.; Yagi, M. *Mol. Cryst. Liq. Cryst.* **1990**, *186*, 167.

- (18) (a) Winke, J. R.; Worsham, P. R.; Schanze, K. S.; Whitten, D. G. *J. Am. Chem. Soc.* **1983**, *105*, 3951–3956. (b) Turro, N. J.; Liu, K.-C.; Chow, M.-F. *Photochem. Photobiol.* **1977**, *26*, 413.
 (19) Guillet, J. *Adv. Photochem.* **1988**, *14*, 91.
 (20) Saphier, S.; Sinha, S. C.; Keinan, E. *Angew. Chem., Int. Ed.* **2003**, *42*, 1378–1381.

Scheme 2. Synthesis of Haptens **6** and **7**

(a) LDA, THF. (b) $\text{BH}_3\text{-SMe}_2$, THF. (c) TsCl, pyridine. (d) LDA, THF. (e) i. chromatographic separation, ii. LiOH, H_2O /methanol/THF.

Scheme 3. Synthesis of Substrates **1a–c**

(a) Mg, Li_2CuCl_4 , THF. (b) DIBAL-H, CH_2Cl_2 . (c) Mg, THF. (d) PCC, diatomaceous earth, CH_2Cl_2 . (e) PTSA, THF, H_2O . (f) KMnO_4 , H_2O , *tert*-butyl alcohol, NaH_2PO_4 .

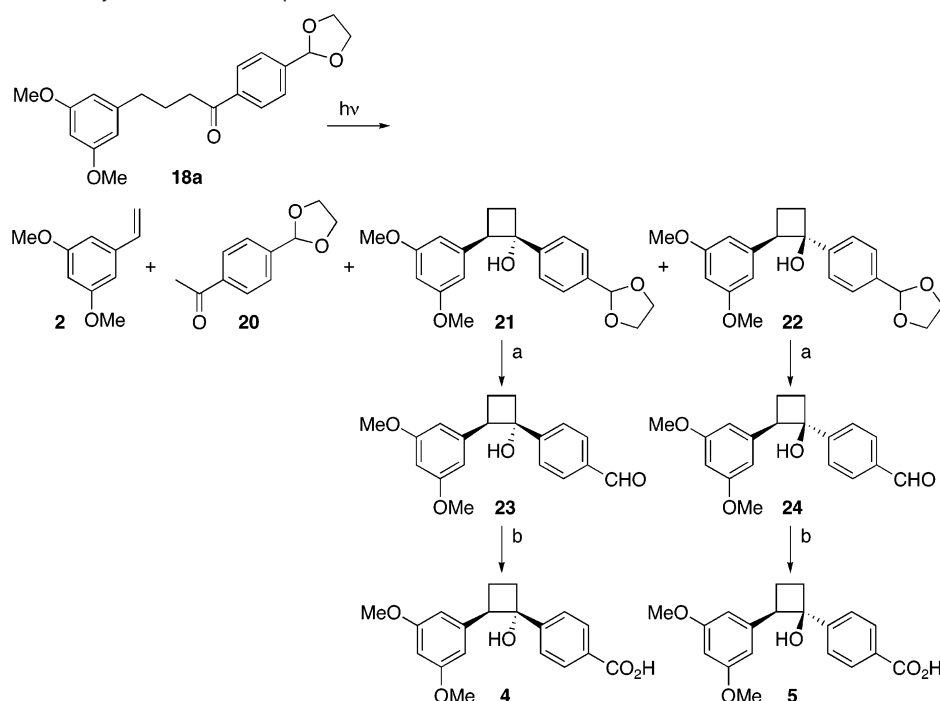
pyridine. Treatment of the latter with LDA afforded oxetanes **12** and **13**, which were separated by column chromatography and then hydrolyzed with aqueous LiOH in THF-MeOH to give the desired haptens, **6** and **7**, respectively.

Substrates **1a–c** were prepared starting from the commercially available chloro or bromo arenes, **14a–b**, and ester **15c**, respectively (Scheme 3). Thus, compounds **14a–b** were converted to the corresponding Grignard reagents and then coupled with ethyl 4-iodobutyrate to produce esters **15a–b**. Compounds **15a–c** were reduced with DIBAL-H to afford the corresponding aldehydes, **16a–c**. The latter were reacted with

a Grignard reagent that was produced from the 4'-bromophenyl-1,3-dioxolane, affording alcohols **17a–c**. Oxidation with PCC yielded the corresponding ketones **18a–c**. The ethylene glycol acetal was hydrolyzed to give keto-aldehyde **19a–c**. Finally, oxidation with KMnO_4 in *tert*-butyl alcohol–aqueous NaH_2PO_4 system²¹ afforded the carboxylic acids **1a–c**.

Authentic samples of the expected cyclobutanol photoproducts, **4** and **5**, were synthesized in very low yields using the Norrish type II reaction as a key step (Scheme 4). Attempts to

(21) Abiko, A.; Roberts, J. C.; Takemasa, T.; Masamune, S. *Tett. Lett.* **1986**, 27, 4537–4540.

Scheme 4. Synthesis of the Cyclobutanols Photoproducts, **4** and **5**

All structures represent relative, not absolute stereochemistry. Compounds **21**, **23**, **4** are referred to as *cis* (formal nomenclature gives *E*) and compounds **22**, **24**, **5** are referred to as *trans*. See text for stereochemical assignments. (a) PTSA, THF, H₂O. (f) KMnO₄, H₂O, *tert*-butyl alcohol, NaH₂PO₄.

irradiate the keto-acid, **1**, or the keto-aldehyde, **19**, failed to produce any detectable amounts of the desired cyclobutanols. We therefore turned to irradiation of the protected keto-aldehyde **18a**, which has a less electron-deficient ketone function¹⁰ Irradiation with a mercury vapor lamp in acetone for several hours produced mainly the fragmentation products, **2** and **20**, along with the diastereomeric cyclobutanols, **21** and **22** (about 5% of each), which were separated by flash chromatography. The acetal function was then hydrolyzed to give aldehydes **23** and **24**, which were oxidized by KMnO₄ to give the desired carboxylic acids, **4** and **5**, respectively.

The stereochemical assignment of the *cis* and *trans* isomers was initially based on the prediction that the *cis* isomer, **4**, would be more polar than the *trans* isomer, **5** (for simplicity, we refer the *cis* and *trans* nomenclature to the relationship between the two aromatic rings, and not to the systematic IUPAC rules). This assumption was later confirmed by comparing the ¹H NMR spectra of **4** and **5** with the reported spectra of *cis*- and *trans*-1,2-diphenylcyclobutanols (the structure of *cis*-1,2-diphenylcyclobutanol was confirmed by an X-ray crystallography).²² The literature spectra, particularly the cyclobutanol methylene signals at 1.8–3.0 ppm matched the analogous signals of compounds **21** and **22**. Furthermore, a Nuclear Overhauser Enhancement (NOE)²³ was observed with our *trans* isomer, **22**. We carried out a 1D NOE experiment and used multiple selective frequency version of NOE, where each line of a multiplet was irradiated for a short time within a narrow bandwidth. The NOE experiment confirmed the assignment of the *trans* stereochemistry, with the benzylic hydrogen at 3.9 ppm exhibiting close

proximity to the hydrogens on both aromatic rings, a situation that was not observed with the *cis* isomer.

Immunization and Screening

The two isomeric haptens, **6** and **7** (in the form of racemic mixtures) were mixed in a 1:1 ratio and the mixture was conjugated to KLH and to BSA using known procedures.^{24a} The KLH conjugate was used to elicit monoclonal antibodies using standard hybridoma technology.^{24b} Preliminary ELISA screening for the best binders of **6** and **7**, using the BSA conjugate,^{24c} afforded a remarkably large number of 800 antibody-producing hybridoma cell lines. Being interested in antibodies that bind the entire substrate molecule in the desired conformation, we have selected for the 60 best binders based on their selective recognition of either **6** or **7**. The selected 60 antibodies were produced in large amounts (30–150 mg) from ascites fluid and then purified by ammonium sulfate precipitation and by protein-G affinity chromatography.

The expected role of the antibodies was to provide an entropic trap for the substrate by strongly binding its productive conformation for cyclization. A prerequisite for catalysis is thus good binding of the antibodies to the substrate. In contrast to nonphotochemical biocatalyzed reactions, where substrate binding to the catalyst is usually indirectly obtained from *K_M* values, in this case no reaction was expected upon binding of the substrate to the antibody in the absence of UV. Therefore, substrate binding could be estimated directly by ELISA. Accordingly, further selection for catalysts using ELISA procedures with the **1**–BSA conjugate allowed for narrowing the 60-member library down to 10 antibodies. Initial catalytic

(22) Forward, P.; Hunter, W. N.; Leonard, G. A.; Palou, J.; Walmsley, D. Watt, C. I. F. *J. Chem. Soc., Perkin Trans* **1993**, 2, 931.

(23) Braun, S.; Kalinowski, H. O.; Berger, S. In "150 and More Basic NMR Experiments: A Practical Course", Wiley-VCH: Weinheim, 1998; p 87–92.

(24) (a) Staros, J. V.; Wright, R. W.; Swingle, D. M. *Anal. Biochem.* **1986**, 156, 220. (b) Goding, J. W. *Monoclonal Antibodies: Principles and Practice*, 2nd ed.; Academic Press: New York 1986. (c) Clark, B.; Engvali, E. In *ELISA: Theoretical and Practical Aspects in Enzyme-Immunoassay*; Maggio, E. T., Ed.; CRC Press: New York, 1980; Chapter 8.

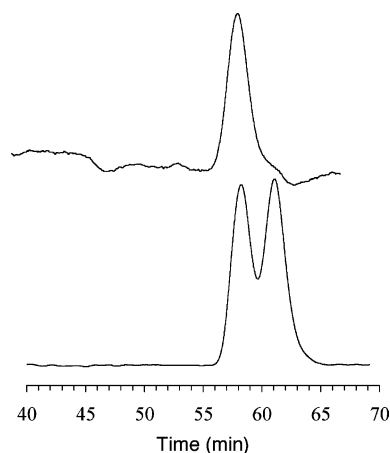


Figure 1. HPLC chromatogram with chiral column of an authentic racemic *cis*-cyclobutanol (bottom) and product of nonracemic photoproduct from the irradiation of substrate in the presence of antibody 20F10 (top).

experiments were performed with each antibody, monitoring both substrate and products by HPLC. Our assumption about direct correlation between binding and catalysis was later corroborated by the finding that three catalysts were discovered within the narrow library of 10 anti-**1** antibodies, while no catalyst was found in the remaining group of 50 antibodies that bind well **6** and/or **7**, but are not good binders of **1**.

Antibody-Catalyzed Yang Cyclization Reaction. Antibody concentration was determined by UV absorbance (OD) at 280 nm,²⁵ using the general formula $OD = X \text{ (mg/mL)} \times 1.4$ and an assumed molecular mass of 150 kDa. Preliminary screening for catalysis was carried out by irradiating the PBS solutions of **1** and antibody in small Pyrex test tubes (3 mm diameter, 4 cm length, using mercury vapor lamp). Three antibodies, 12B4, 20F10, and 21H9, were found to catalyze the formation of the *cis*-cyclobutanol, **4**, whose relative stereochemistry was determined by comparison (¹H NMR, MS, UV, and HPLC) with authentic synthetic samples.

Quantitative analysis of all reaction mixtures (substrate + 4 possible photoproducts) was carried out by HPLC using a gradient of acetonitrile and water containing 0.1% trifluoroacetic acid (TFA). Each antibody was used at the highest available concentration in PBS (pH 7.4). A solution of the substrate in acetonitrile (10 μ L) was added to the antibody solution (90 μ L) to reach a final substrate concentration of 50 μ M. Keeping the resultant mixture at room temperature for 24 h did not result in any apparent reaction. In control experiments the substrate was irradiated in either acetone or benzene or PBS (pH 7.4), producing only fragmentation products and no detectable cyclization products. Purging argon into the mixture prior to the irradiation for 3 to 15 min showed no effect on results. In another control experiment antibodies were irradiated without substrate, exhibiting no detectable products by HPLC. No reaction was observed in the dark either in the presence or absence of antibodies.

Enantioselectivity and Kinetic Studies. The opportunity of achieving enantioselective Yang cyclization is of particular interest because stereochemical control over reactions that involve radical intermediates is generally difficult to attain. We used HPLC with a chiral column to measure the enantioselectivity of the antibody-catalyzed photochemical cyclization. The

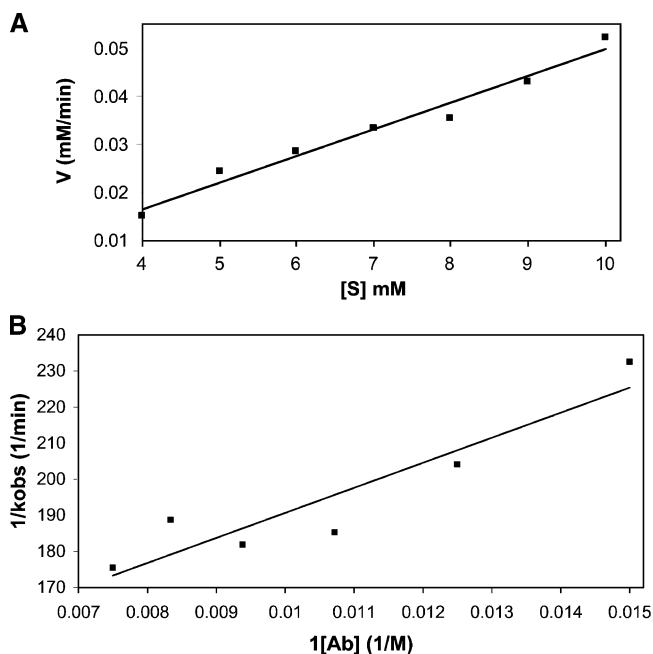


Figure 2. A. Initial rates of product formation under conditions of excess antibody give a pseudo-first-order rate constant: k_{obs} . B: A double reciprocal plot of k_{obs} obtained by a series of kinetic measurements vs antibody concentration, providing the values of k_{cat} and K_M .

chromatograms (Figure 1) were compared with those of an authentic, racemic mixture of **4**, which was synthesized independently. Interestingly, all three antibodies produced **4** with the same relative stereochemistry (*cis*) but with yet unknown absolute configuration (antibody, ee): 20F10, 96%; 12B4, 80%; 21H9, 78%. The most enantioselective antibody, 20F10, also yielded the highest cyclization/fragmentation ratio (70:30) under irradiation at 312 nm. In these experiments, 2 mL Pyrex vials containing the antibody and substrate solution were placed on top of a 312 nm emitting Vilber Lourmat UV lamp, and the progress of the reaction was monitored by HPLC.

Antibody 20F10 was selected for further characterization and kinetic studies. Under low antibody concentrations, the background photochemical cleavage reaction became dominant. This precluded measurements of the cyclization initial rates under Michaelis–Menten approximation, where low catalyst concentrations relative to substrate loads are normally used to determine the kinetic parameters (k_{cat} and K_M). To circumvent this problem we turned to an alternative model, using excess catalyst with constant substrate concentration. Under such conditions, rate constants were obtained from a series of pseudo-first-order kinetic data, which were modeled according to the general format of Michaelis–Menten, as described by Klotz (Figure 2).²⁶

$$1/k_{\text{obs}} = K_M/k_{\text{cat}} * [\text{Ab}]_0 + 1/k_{\text{cat}}$$

Obviously, the rate constant is highly dependent on the flux of light. For example, when using a 150W–Xenon lamp the reaction was complete within 10 s. This high k_{cat} made it technically difficult to obtain accurate results. We therefore used a weaker 75W–Xenon lamp to delay the reaction over a time span of 20 min. Under these conditions, we obtained the values

(25) Peterson, G. L. *Methods. Enzymol.* **1983**, 91, 95.

(26) Suh, J.; Scarpa, I. S.; Klotz, I. M. *J. Am. Chem. Soc.* **1976**, 98, 7060–7064.

of $k_{\text{cat}} = 0.008 \pm 0.001 \text{ min}^{-1}$ and $K_M = 58 \pm 13 \mu\text{M}$. Obviously, much higher values of k_{cat} could be obtained with more intense UV lamps. Noticeably, no cyclization products were detected in the absence of the antibody.

To evaluate the antibody catalytic efficiency over multiple turnovers, the antibody was recycled several times by dialysis and its activity was examined. The concentration of the antibody after each dialysis step was determined by UV absorbance. To minimize background the photochemical reaction was performed in each cycle with equal concentrations of antibody and substrate. No reduction in activity was observed after five cycles, indicating that the protein active site is remarkably stable under the photochemical conditions. The stability of antibodies under conditions of UV radiation seems to be a general phenomenon.²⁷ Moreover, the ability of the antibody active site to handle reactive intermediates, including free radicals, carbonium ions²⁸ and reactive oxygen species,²⁷ is of particular significance to the general fields of biocatalysis and immunology. Total product formation amounted to more than 3-fold the initial concentration of the antibody. This observation, together with the catalyst stability suggests that, in principle, the catalyst could be immobilized and used in a flow system for continuous synthesis of the photoproduct.²⁹

Wavelength Dependence. The dependence of cyclization efficiency on the irradiation wavelength was examined in a series of experiments in which the initial cyclization rate was measured by irradiation at various wavelengths within the range of 245–340 nm. Monochromatic irradiation was achieved using a monochromator with a 5 nm slit. Relative intensities were determined using a thermophile absorber, which make use of the heating effect of light absorbed by a blackened surface. These sensors are quite sensitive and give an absolute calibration of the light intensity.³⁰ The thermophile had a linear response to light at the range of the measured wavelength. Relative intensities were accounted for by different irradiation times, allowing for the measurement of the initial rates. As can be seen in Figure 3, the relative rates followed quite faithfully the antibody absorption spectrum, with a red-shift of approximately 10 nm. This observation suggests that an active site tryptophan could act as a sensitizer that transfers the light energy to the substrate.^{8a} By contrast, the fragmentation efficiency was found to follow the absorption spectrum of the substrate ($\lambda_{\text{max}} = 250 \text{ nm}$). The different wavelength dependence of the two reaction routes could be exploited to optimize the cyclization yield. Indeed, the cyclization/fragmentation ratio was increased from 37:63 at 240 nm to 70:30 at 312 nm. Generally, it is known that unsubstituted phenyl ketones absorb UV radiation in the UV–B (very weak band at 280–315 nm) and the UV–C (200–280 nm) spectral regions. There is a solvent effect on the spectrum when going from organic solvent to water, with a blue shift of the weakly absorbing $n\text{-}\pi^*$ transition in the UV–B region and a red shift of the $\pi\text{-}\pi^*$ transition.³¹ This phenomenon was observed in the absorption spectrum of substrate **1a**.

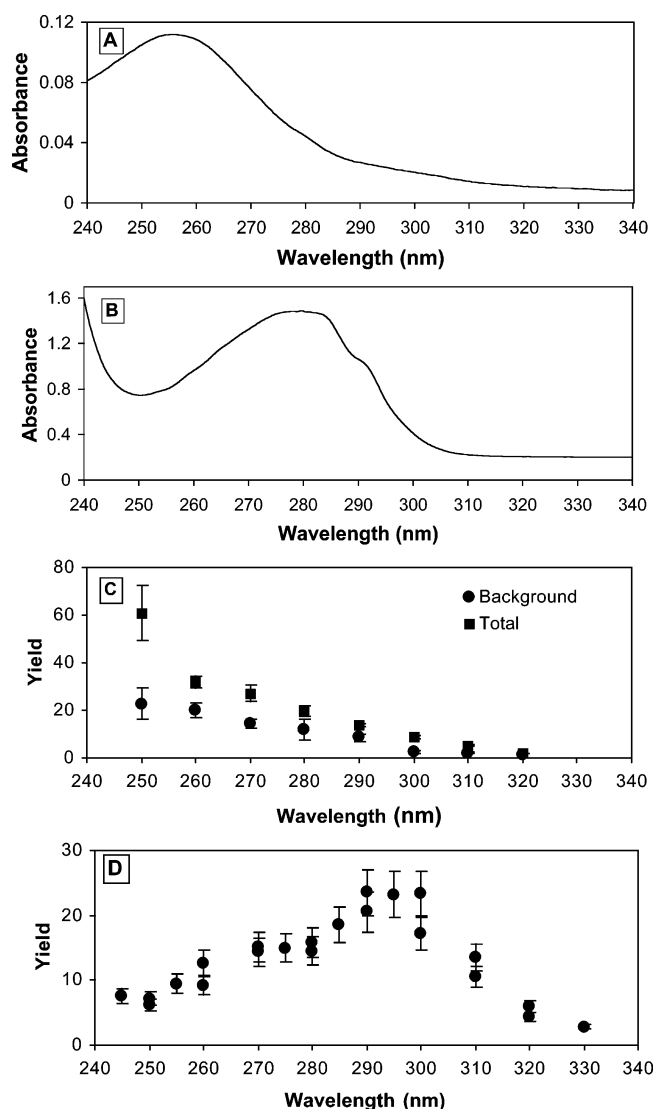


Figure 3. A. Absorption spectrum of substrate **1a** (10^{-5} M in PBS, pH 7.4 in the absence of antibody). B. Absorption spectrum of antibody 20F10 (PBS, pH 7.4). C. Relative yields of fragmentation as a function of wavelength (background refers to reaction in the absence of antibody). D. Relative yields of cyclization with antibody 20F10 as a function of wavelength.

Binding Constants. Since substrate **1** is inert in the dark, it is possible to directly measure its binding constants to the antibody. The Isothermal Titration Calorimetry (ITC) technique, which monitors the release of thermal energy upon binding, was found to be a convenient tool for this purpose.³² The antibody was dialyzed into freshly prepared PBS (pH 7.4). Solutions of substrates and haptens were also prepared in the same buffer at 8.5-fold higher concentration. Remarkably, the binding constants, K_a (M^{-1}), which were obtained from the titration diagrams (Table 1), show that antibody 20F10 binds the substrate **1a** stronger than it binds either the *cis*- or the *trans*-hapten, **6** or **7**. Furthermore, although the antibody selectively catalyzes the formation of the *cis*-cyclobutanol, **4**, it binds the *trans*-oxetane, **7**, more tightly than the *cis*-isomer, **6**. This remarkable observation, which agrees with the more qualitative ELISA experiments described above, could be attributed to the molecular flexibility of **1a**. The optimal binding conformation

(27) Wentworth, A. D.; Jones, L. H.; Wentworth, P., Jr.; Janda, K. D.; Lerner, R. A. *Proc. Natl. Acad. Sci. U.S.A.* **2000**, *97*, 10930–10935.

(28) Hasseroth, J.; Janda, K. D.; Lerner, R. A. *J. Am. Chem. Soc.* **2000**, *122*, 40–45.

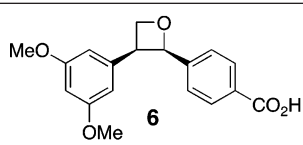
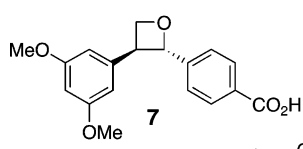
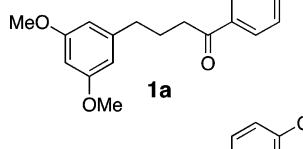
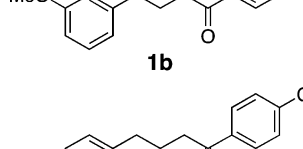
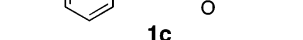
(29) Shabat, D.; Grynszpan, F.; Saphier, S.; Turniansky, A.; Avnir, D.; Keinan, E. *Chem. Mater.* **1997**, *9*, 2258.

(30) Wayne, C. E.; Wayne, R. P. In *Photochemistry*; Oxford Science Publications: Oxford, 1996.

(31) Zepp, R. G.; Gumz, M. M.; Miller, W. L.; Gao, H. *J. Phys. Chem. A* **1998**, *102*, 5716–5723.

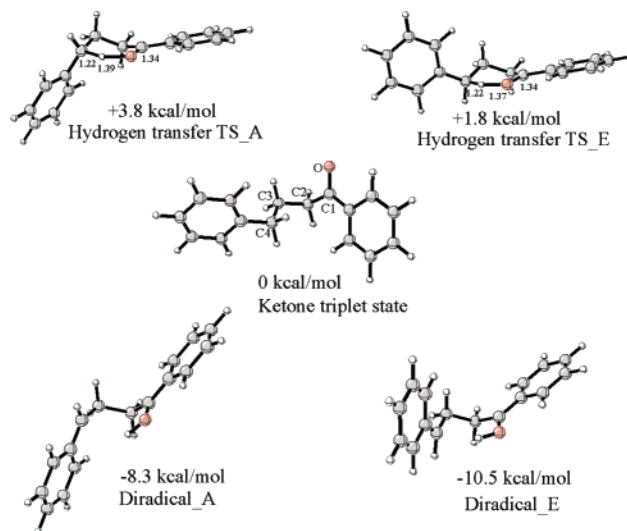
(32) Livigstone, J. R. *Nature* **1996**, *384*, 491–493.

Table 1. Binding Constants of Haptens and Substrates to Antibody 20F10 by ITC

	K_a (M^{-1})
 6	$5.9 (\pm 0.8) \times 10^4$
 7	$2.1 (\pm 0.1) \times 10^5$
 1a	$1.9 (\pm 0.1) \times 10^6$
 1b	$1.2 (\pm 0.2) \times 10^4$
 1c	< 5000

of **1a** probably does not follow accurately the rigid structure of either **6** or **7**, but rather adopts an intermediate conformation that is suitable for photocyclization. It has been proposed that cleavage of the 1,4-biradicals requires good overlap between the radical-containing p-orbitals and the C2–C3 bond.³³ In contrast, cyclization would predominate in the absence of such alignment, provided that the C1 and C4 orbitals are still within reasonable overlap. Thus, it is conceivable that the protein imposes conformational constraints on the substrate that enforces preferential cyclization over fragmentation.

Substrate Substituent Effect. It has been shown for the Norrish type II reactions that electron withdrawing substituents at the γ -carbon of a ketone substrate decreases the rate of hydrogen abstraction from that carbon (*meta*-methoxyphenyl substituent is electron withdrawing, $\sigma = 0.10$).^{34,35} However, correlation of hydrogen abstraction rates and total quantum yields does not necessarily exist due to disproportionation of the diradical intermediate. Lewis bases such as alcohol and water are known to inhibit disproportionation to regenerate the ketone.³⁶ Since the reaction medium in the background experiments consisted of an aqueous buffer, disproportionation is generally expected to be retarded for all substrates. Thus, it seemed possible that in our case, electron-withdrawing substituents at γ -carbon would indeed reduce the overall quantum yield of the Norrish type II reaction. Hence, removal of one or two aromatic methoxy groups from substrate **1** (**1b** and **1c**, respectively) was expected to enhance the quantum yield of the Norrish

**Figure 4.** Relative energies on the triplet surface of the ketone, H-transfer transition states and diradical intermediates at the B3LYP/6-31G* level.

type II reaction in the background. Irradiation of the three substrates in solution with and without antibody, under the same conditions, confirmed this expectation, as determined by monitoring the fragmentation products, with the relative rates for substrates **1a**, **1b**, **1c** being 1:2:6, respectively.

On the other hand, the aromatic methoxy groups in the substrate apparently play a crucial role in binding to the antibody, as can be seen from the ITC binding constants of **1a–c** (Table 1). Binding of the monomethoxy substrate, **1b**, by antibody 20F10 is 2 orders of magnitude weaker than the binding of **1a**. Binding of the unsubstituted substrate, **1c**, was practically too low to be measured by the ITC. It could only be estimated that the binding constant is lower than 5000 M^{-1} . These differences are also manifested in the relative cyclization efficiency with these substrates. The relative rates of formation of *cis*-cyclobutanol from substrates **1a**, **1b**, and **1c**, in the presence of antibody 20F10 were found to be 8:2:1, respectively, probably reflecting binding efficiency rather than other substituent effects, and showing an opposite trend to that expected from the electronic effects of the substituents.

Quantum Mechanical Calculations of Transition States.

The photochemical reaction potential surface of the parent system was first explored in the gas phase. Figure 4 shows the computed reaction pathway of the γ -hydrogen abstraction of the triplet excited ketone at the UB3LYP/6-31G* level with the GAUSSIAN 98 package.³⁷ The hydrogen transfer transition state has a chairlike conformation. Depending on the axial or equatorial positions of the phenyl group relative to the six-membered hydrogen transfer core, there are two transition states named TS_A and TS_E, respectively. The π orbitals of one phenyl group align with the C–H–O bond while the other

- (33) Wagner, P. J.; Kemppainen, A. E. *J. Am. Chem. Soc.* **1968**, *90*, 5896–5897.
 (34) March, J. In *Advanced Organic Chemistry*, 4th ed.; John Wiley & Sons: New York, 1992; p 280.
 (35) Wagner, P. J. *Acc. Chem. Res.* **1971**, *4*, 168–177.
 (36) (a) Wagner, P. J. *J. Am. Chem. Soc.* **1967**, *89*, 5898–5901. (b) Wagner, P. J.; Kochevar, I. E.; Kemppainen, A. E. *J. Am. Chem. Soc.* **1972**, *94*, 7489–7494.

- (37) Frisch, M. J.; Trucks, G. W.; Schlegel, H. B.; Scuseria, G. E.; Robb, M. A.; Cheeseman, J. R.; Zakrzewski, V. G.; Montgomery, J. A., Jr.; Stratmann, R. E.; Burant, J. C.; Dapprich, S.; Millam, J. M.; Daniels, A. D.; Kudin, K. N.; Strain, M. C.; Farkas, O.; Tomasi, J.; Barone, V.; Cossi, M.; Cammi, R.; Mennucci, B.; Pomelli, C.; Adamo, C.; Clifford, S.; Ochterski, J.; Petersson, G. A.; Ayala, P. Y.; Cui, Q.; Morokuma, K.; Malick, D. K.; Rabuck, A. D.; Raghavachari, K.; Foresman, J. B.; Cioslowski, J.; Ortiz, J. V.; Stefanov, B. B.; Liu, G.; Liashenko, A.; Piskorz, P.; Komaromi, I.; Gomperts, R.; Martin, R. L.; Fox, D. J.; Keith, T.; Al-Laham, M. A.; Peng, C. Y.; Nanayakkara, A.; Gonzalez, C.; Challacombe, M.; Gill, P. M. W.; Johnson, B. G.; Chen, W.; Wong, M. W.; Andres, J. L.; Head-Gordon, M.; Replogle, E. S.; Pople, J. A. *Gaussian 98*, Revision A.9; Gaussian, Inc.: Pittsburgh, PA, 1998.

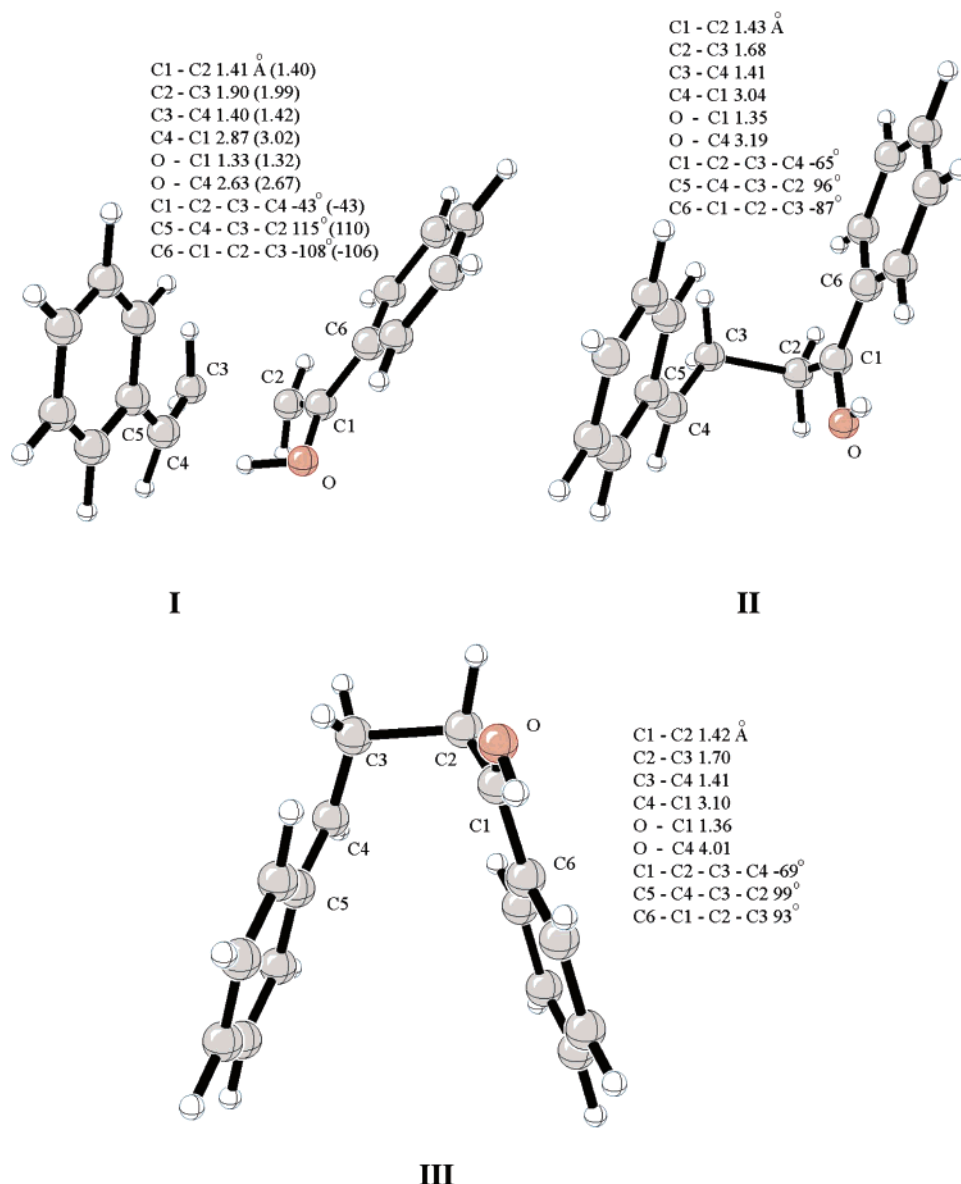


Figure 5. Computed geometry of the pseudo-*trans*-fragmentation transition states, **I** and **II**, and pseudo-*cis*-fragmentation transition state, **III**, at the PM3 and UB3LYP/6-31G* (in parentheses) level.

phenyl group is in conjugation with the carbonyl group in both transition states. The γ -hydrogen transfer has a low activation barrier (~ 2 – 4 kcal/mol). The distances between the oxygen and the γ -hydrogen are 1.39 and 1.37 Å, respectively. The C–H distance is 1.22 Å in both TS_A and TS_E. The equatorial diradical intermediate is more stable than the axial counterpart by 2.0 kcal/mol, which comes almost entirely from the free energy difference of the phenyl-substituted axial/equatorial cyclohexene conformers (2.9 kcal/mol).³⁸ The following studies concentrate on the path leading to the equatorial diradical intermediate.

The two transition states that originate from the equatorial singlet diradical intermediate to fragmentation and cyclization products were examined. Three possible fragmentation transition states were found at both PM3 and UB3LYP/6-31G* level. There are two possible fragmentation pathways depending on the O–C1–C2–C3 dihedral angle. Two transition states are

associated with the 90° (cis-fragmentation) pathway and one transition state with the 270° (trans-fragmentation) pathway according to the relative positions of the two phenyl groups.

Figure 5 shows the geometries of the three fragmentation transition states, **I–III**, at PM3 and UB3LYP/6-31G* levels. PM3 predicts that the pseudo-*trans* structure, **I**, has a relatively loose geometry comparing to the one predicted by UB3LYP/6-31G*. The two methods agree very well in most of the key geometry descriptors. One major difference between the two methods is the C1–C4 distance, which is 2.87 Å predicted by PM3 and 3.02 Å by UB3LYP/6-31G*. For the rest of transition states, single point energy calculations were performed at UB3LYP/6-31G* level based on PM3 geometry optimization. All three transition states were found to be less stable than the diradical intermediate. This also indicates that fragmentation happens after formation of the diradical intermediate.

I is the most stable transition state with an activation barrier from the singlet diradical intermediate of 8.1 kcal/mol comparing to 9.4 kcal/mol for **II** and **III**. This energy advantage mainly

(38) Kasunic, L. B.; Evoy, I. L.; Sukenik, C. N. *J. Org. Chem.* **1981**, *46*, 1969–1970.

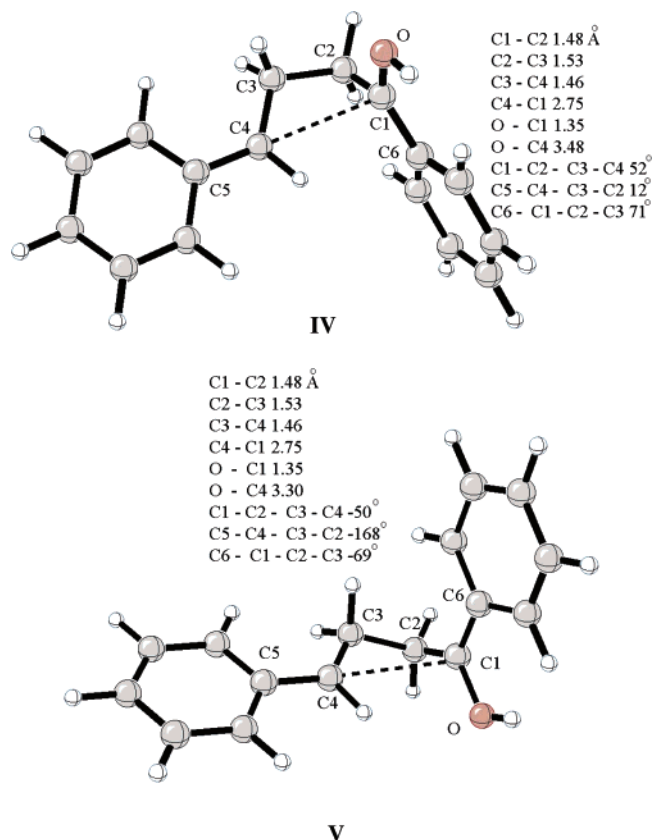


Figure 6. Computed geometries of the pseudo-*trans*-cyclization transition state, **IV**, and pseudo-*cis*-cyclization transition state, **V**, at the PM3 level.

comes from a noticeable hydrogen bond between the carbonyl and C4. As a result, **I** has a longer C2–C3 distance (1.90 Å) and a shorter C1–C4 distance (2.87 Å) in comparison to 1.68 Å and 3.04 Å in **II**, respectively. In both **I** and **II**, C1–C2 and C3–C4 bonds show partial double bond characteristics. The dihedral angle of the four-membered carbon backbone is nonplanar at –43°. Two p orbitals of the radical centers line up with the C2–C3 bond. Especially in **II**, the two p orbitals are almost parallel given that dihedral angles of C5–C4–C3–C2 and C3–C2–C1–C6 are close to 90°.

Transition state **III** resembles transition state **II** in terms of both energy and geometry except that in **III** the two phenyl groups are facing one another (Figure 5), creating some steric repulsion between them. Yet, **III** is still energetically equivalent to **II**. Both radicals are positioned away from one another (C1–C4 3.1 Å), in line with the breaking C2–C3 bond. However, the nonplanarity of the C1–C2–C3–C4 backbone prevents direct interactions between two radical p orbitals.

The pseudo-*trans* and pseudo-*cis* cyclization transition states, **IV** and **V** have activation energies of 9.2 and 10.2 kcal/mol, respectively. In both **IV** and **V**, the four bond lengths of the C1–C2–C3–C4 backbone are identical (Figure 6). The C2–C3 bond in both has normal single bond length of 1.53 Å. The C2–C3 is significantly shorter (1.53 Å) than in fragmentation transition states (between 1.68 and 1.9 Å). The forming bond C1–C4 distance is decreased from 3.13 Å in the diradical intermediate to 2.75 Å in the cyclization transition state, as compared with the distance of 2.87 Å in **I**. Both p orbitals do not maintain ideal alignment with C2–C3 bond, as indicated by the dihedral angles ranging from 12° to 21°.

20F10 (1IAI) light chain:

DIVMTQSHKFMSTSVGDRVSITCKASQDVSTTVAWYQKPGQSPKLLIYSASYRYTGVP
 DIVMTQSHKFMSTSVGDRVSITCKASQDVSTAVAWYQKPGQSPKLLIYSASYQYTGVI

DRFTGSGSGTDFTFTISSVQAEDLAVYYCQHYSTPTFGGGTKLEIKR
 DRFTGSGSRTDFTFTISVQAEDLAVYYCHQHYSTPTFGSGTKLEIKR

20F10 (1F3D) heavy chain:

EVQLQQSGPELVKPGASMKISCKTSGYSFTGYTMNWIKQSHGNLEWILINPSNGGTT
 EQLQQSGPELVKPGASVSKSGYSFTDYNIHWKQSHGKLEWIVPYSGGTT

NQKFKGKATLTVDKSSSTAYMELLSLTSEDASVYYCARVGYITNYWGQGTTLTVS
 NQKFKGKATLTVDKSSSTAMELLSLTSEDASVYYCAVDYDGVYWGQGTTLTVS

Figure 7. Sequence alignment of 1IAI and 1F3D (blue) with 6 complementarity determining regions (CDR) (yellow); mismatched residues are shown in pink (in non-CDR) and green (in CDR).

Excellent orbital alignment between the breaking C2–C3 bond and the two radical p orbitals drive the fragmentation reaction toward the formation of two unsaturated products. On the other hand, the cyclization pathway requires good overlap between two radical p orbitals and deviation from good alignment with the C2–C3 bond.^{33,39} The diradical intermediate generally lies on a relatively flat potential surface. The activation energies for both fragmentation and cyclization processes are relatively small. The activation energies for the fragmentation via transition state, **I**, and for cyclization via the pseudo-*trans* transition state, **IV**, are 8.1 and 9.2 kcal/mol, respectively.

Single point energy calculations on the fragmentation and cyclization transition states with the carboxylic acid and two methoxy substituents were conducted at UB3LYP/6-31G* level based on the PM3 optimized geometries. The activation enthalpy of the fragmentation pathway is more favored than the cyclization by 7.9 kcal/mol. These results explain the experimental observation of exclusive formation of the fragmentation products in the uncatalyzed photochemical reaction of **1a**. Complete transition state geometry optimizations at UB3LYP/6-31G* level were very time-consuming and could not be completed in a reasonable period of time.

Homology Modeling and Docking. To understand the role that the antibody plays in the product redistribution, we built a 3D model using the BLAST database.⁴⁰ 20F10 light chain and heavy chain were searched with BLASTP separately.⁴¹ Antibodies 1IAI and 1F3D were found to be among the most homologous sequences to the light chain and heavy chains of 20F10, with 94% and 78% sequence identities, respectively (Figure 7). The Chothia canonical class definitions⁴² were used to identify the six complementarity determining regions (CDRs). 1IAI was found to resemble the 20F10 light chain very well. There are only six mismatches between 1IAI and 20F10 light chain sequences and only four of them are in the CDR regions. On the other hand, 20F10 heavy chain was more difficult to model due to a larger number of amino acid mismatches (Figure 7). This could lead to inexact prediction of the three-dimensional structure. Nevertheless, a 3D 20F10 structure was built by overlapping 1IAI and 1F3D heavy chains and light chains with

(39) Braga, D.; Chen, S.; Filson, H.; Maini, L.; Netherton, M. R.; Patrick, B. O.; Scheffer, J. R.; Scott, C.; Xia, W. *J. Am. Chem. Soc.* **2004**, *126*, 3511–3520.

(40) <http://www.ncbi.nih.gov/BLAST>.

(41) Altschul, S. F.; Madden, T. L.; Schäffer, A. A.; Zhang, J.; Zhang, Z.; Miller, W.; Lipman, D. J. *Nucleic Acids Res.* **1997**, *25*, 3389–3402.

(42) Chothia, C.; Lesk, A. M. *J. Mol. Biol.* **1987**, *196*, 901.

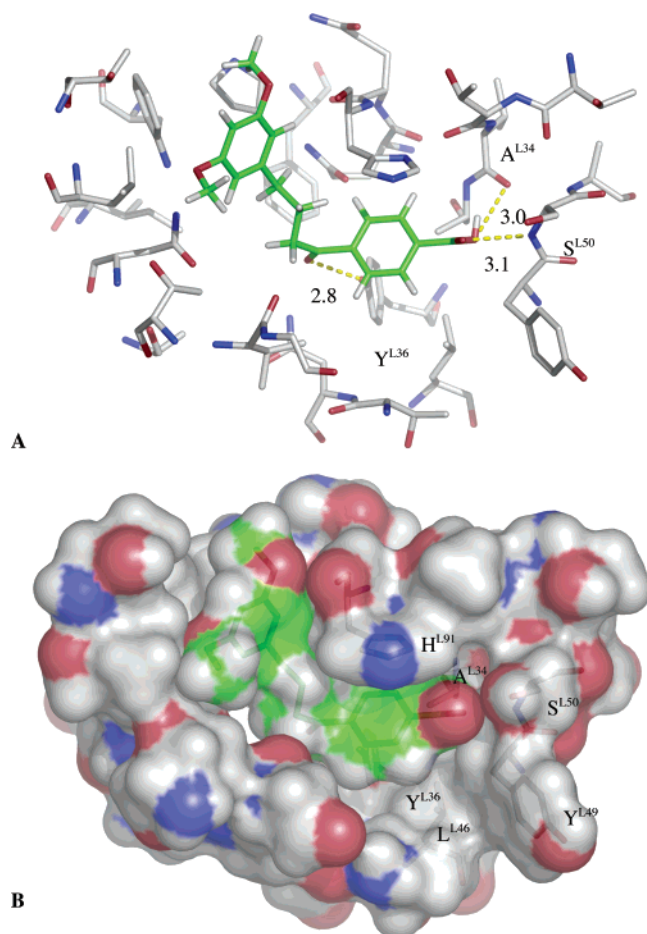


Figure 8. Flexible substrate docked in antibody 20F10 combining site (a) and surface representation (b).

each other. Then 1IAI light chain and 1F3D heavy chain were combined into a structure, which is considered as antibody 20F10 homology structure. The new sequence was then corrected and some amino acids were mutated according to 20F10 sequence. The final structure was obtained after minimization with AMBER 7.0.⁴³

Docking of substrate, haptens, and transition states was performed with Autodock 3.0.⁴⁴ The four atoms of the oxetane ring in the haptens or the cyclobutanol ring in the transition states were chosen as root atoms. The total number of degrees of freedom was six, including single bond rotation between the aromatic rings and their substituents—the carboxylic acid and two methoxy groups. The receptor was chosen to be rigid. The binding free energies predicted by docking experiments were used to rank the binding affinities to the antibody. All docking results are shown in the Figures from the same viewpoint.

Substrate docking with all single bond flexibilities generates only one dominant binding mode (Figure 8A) with the binding free energy being -8.5 kcal/mol, which agrees with the measured binding constant of 10^{-6} M between 20F10 and substrate **1a** (vide supra). The carboxylic acid in **1a** forms two

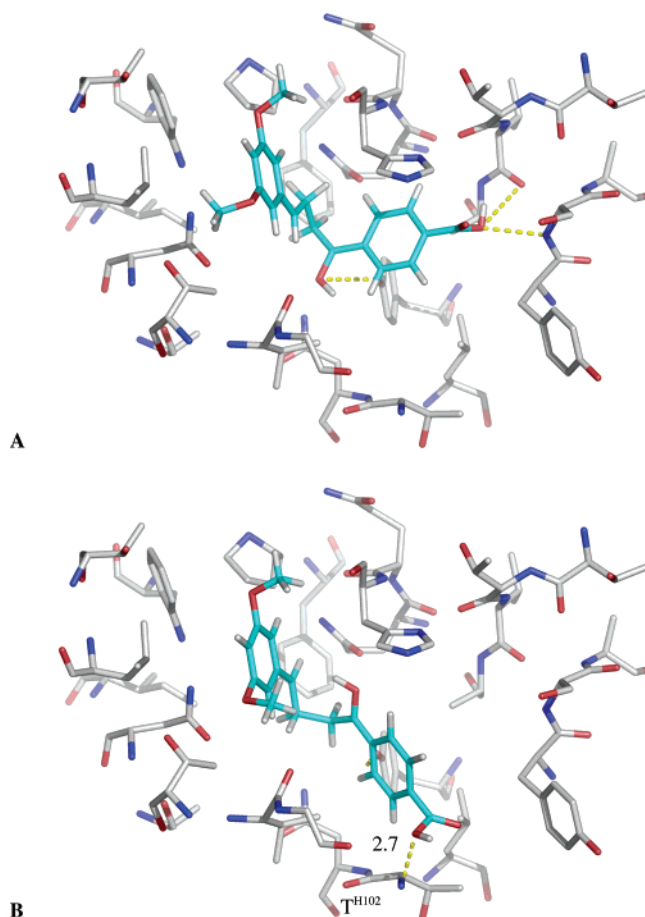


Figure 9. Cyclization, A, and fragmentation transition state, B, docked in antibody 20F10 combining site.

hydrogen bonds with Ser L50 and Ala L34 amide at about 3.0 Å. A third hydrogen bond is formed between the carbonyl group and Tyr L36 at 2.8 Å. His L91 along with Ala L34, Tyr L36, Leu L46, and Ser L50 define a relatively narrow corridor and shallow concave site at the right side of the combining site and confine the phenyl group in the middle of the combining site (Figure 8B). These interactions indicate that **1a** is bound in a single, highly preferred conformation within the antibody combining site.

The binding free energies of the cyclization and fragmentation transition states were found to be -7.9 and -7.3 kcal/mol, respectively. The cyclization transition state adopts a binding mode that is reminiscent of the substrate binding, including hydrophobic interactions with His L91 and Tyr L36 and hydrogen bonding with Ser L50, Ala L34, and Tyr L36 (Figure 9A). In contrast, the antibody was found to bind the fragmentation transition state in a completely different manner (Figure 9B). The two phenyl groups slice the combining site diagonally leaving formation of a hydrogen bond between the carboxylate acid and Thr H102 backbone amide at 2.7 Å. A strenuous conformational change is needed in order to force the bound substrate to adopt the conformation of the fragmentation transition state. Consequently, the extraordinary resemblance between the binding modes of the substrate and the cyclization transition state, particularly in comparison with the poor resemblance to the fragmentation transition state, could explain the origin of catalysis of the cyclization reaction by antibody 20F10.

(43) Case, D. A.; Pearlman, D. A.; Caldwell, J. W.; Cheatham, T. E., III.; Wang, J.; Ross, W. S.; Simmerling, C. L.; Darden, T. A.; Merz, K. M.; Stanton, R. V.; Cheng, A. L.; Vincent, J. J.; Crowley, M.; Tsui, V.; Gohlke, H.; Radmer, R. J.; Duan, Y.; Pitera, J.; Massova, I.; Seibel, G. L.; Singh, U. C.; Weiner, P. K.; Kollman, P. A. 2002, AMBER 7, University of California, San Francisco.

(44) Morris, G. M.; Goodsell, D. S.; Halliday, R. S.; Huey, R.; Hart, W. E.; Belew, R. K.; Olson, A. J. *J. Comput. Chem.* **1998**, *19*, 1639–1662.

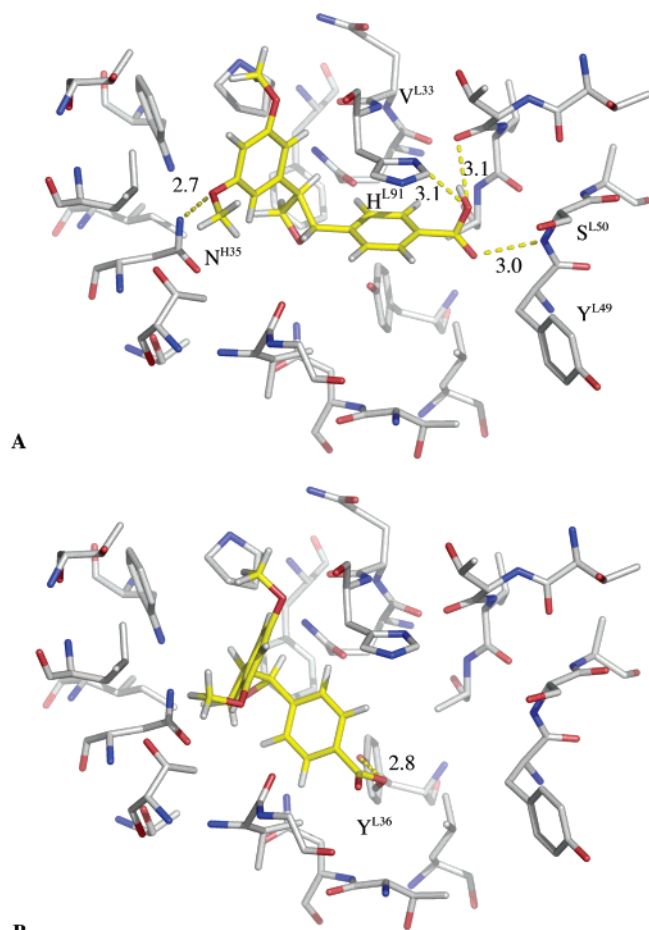


Figure 10. *Trans*, A, and *cis*, B, haptens docked in antibody 20F10 combining site.

The model of antibody 20F10 was found to bind one enantiomer of the *trans*-hapten, **7**, and one enantiomer of the *cis*-hapten, **6**, with the computed binding free energies being -8.1 and -6.9 kcal/mol, respectively (Figure 10). The carboxylic acid of **7** forms three hydrogen bonds with Ser L50, Val L33 backbone and His L91 at about 3.0 Å (Figure 10A). One methoxy group forms a hydrogen bond with Asn H35 at 2.7 Å. There is also one hydrogen bond between the oxetane oxygen and Tyr L36. His L91 also stacks with one phenyl ring in the hapten. The *cis*-hapten, **6**, has a different binding mode in that there is only one hydrogen bond between the hapten and the antibody and no π stacking. The phenyl ring on the right side is away from the cleft formed by His L91 and Tyr L36 (Figure 10B). These results correlate well with the observed 10-fold preference for binding of the *trans*-hapten by antibody 20F10.

Experimentally, the fragmentation efficiency was found to follow the substrate absorption spectrum (vide supra). In contrast, the cyclization pathway peaks at 290 nm, which is closer to the antibody absorption curve that has a maximum at 280 nm. This observation suggests that a tryptophan residue in the antibody combining site could function as a sensitizer, thus promoting the cyclization reaction. Our modeling studies established that there is indeed one tryptophan, Trp H47, in the antibody combining site. However, the ketone group in both substrate and transition states is positioned relatively far away from Trp H47. Alternatively, Tyr L36 and His L91, which are positioned in close proximity to the substrate, could also function

as photosensitizers at the UV region (250 – 290 nm). The π – π stacking between His L91 and one phenyl group of the cyclization transition state could also explain the small red-shift from the antibody absorption to the cyclization photoexcitation.

Conclusions

Although many notions have been put forth to explain enzymatic catalysis involving substrates in their ground state, much less is known about how specific binding energy can be effectively used to control physical and chemical processes of excited-state molecules. In this work, the first antibody-catalyzed Yang (Norrish type II) cyclization has been achieved with antibodies that were elicited against *cis*- and *trans*-2,3-diaryl-oxetanes. The photocyclization of 1,4-diarylbutan-1-one produced a single stereoisomer of *cis*-1,2-diarylcyclobutanol with very high enantioselectivity. Remarkably, the cyclization pathway dominated in the presence of antibody 20F10, producing up to 70% cyclobutanol, while the background photochemical reaction in the absence of the antibody yielded only fragmentation products. The 20F10-catalyzed reaction was studied in detail, exploring its selectivity, substituent effects, substrate, and hapten binding, kinetic parameters and irradiation wavelength dependence.

The experimental work was complemented by theoretical studies that explain the observed selectivity. Transition states for the fragmentation and cyclization pathways were located with quantum mechanical calculations, showing that both fragmentation and cyclization pathways with the parent, unsubstituted substrate have similar activation energy. For the substituted substrate used in the experiments, however, fragmentation is significantly favored over cyclization. The antibody sequence was elucidated and a homology model of antibody 20F10 was built using the BLAST technology to locate highly homologous light and heavy chains, which were then modified to the 20F10 sequence. Detailed docking studies on hapten, substrate and transition state binding indicated a binding mode that is very similar for the substrate and the cyclization transition state, but differs for the fragmentation transition state. The effectiveness of 20F10 arises from the preference to bind the substrate in a conformation that can easily undergo only the normally less favored cyclization from its excited state. Antibody catalysis probably involves dual effect of stabilizing the productive conformation of the substrate as well as light harvesting and energy transferring. Several residues, including Trp H47, have been identified that could function as sensitizers for the photocyclization process.

Experimental Section

General Methods. ^1H NMR spectra were recorded on a Bruker AM 200 spectrometer, operating at 200 MHz using CDCl_3 as a solvent (unless otherwise specified). EI–MS spectra were measured on a Finnigan MAT-711 spectrometer. CI–MS spectra were measured on a Finnigan TSQ-70 GCMS–CI linked to a Varian GC equipped with a DB-5ms capillary column. UV–vis spectra were recorded on a Shimadzu UV-1601 spectrometer. Quartz Ultra micro UV Spectrophotometer cuvettes from Sigma-aldrich C-9792 were used for measuring antibodies concentrations. Irradiation experiments performed with cuvettes were carried out in Fischerbrand 0.100 cm, SCC 282 cuvettes. TLC was performed on glass sheets precoated with silica gel (Merck, Kieselgel 60, F254, Art. 5715). Column chromatographic separations

were performed on silica gel (Merck, Kieselgel 60, 230–400 mesh, Art. 9385) under pressure. THF was dried and distilled over sodium/benzophenone. HPLC analyses were carried out with a Merck-Hitachi Lachrom system equipped with a L-7100 pump, L-7400 UV-vis detector and D-7000 system manager using Supelco RP LC-18 analytical column.

2-(3',5'-Dimethoxyphenyl)-3-hydroxy-3-(4"-methoxycarbonylphenyl)propanoic acid, 8, 9. A Solution of LDA was prepared by dropwise addition of *n*-BuLi (2.5 M, 8.8 mL, 22 mmol) to a solution of diisopropylamine (4.7 g, 24 mmol) in dry THF (30 mL) at 0 °C. A Solution of the 3,5-dimethoxy phenyl acetic acid (1.96 g, 10 mmol) in dry THF (5 mL) was added dropwise to the LDA solution at –78 °C and stirring was continued for 2 h while warming from –78 °C to 0 °C. A solution of methyl 4-formyl-benzoate (1.64 g, 10 mmol) in dry THF (5 mL) was added to the reaction mixture at –78 °C. After 0.5 h, the reaction was worked up by addition of saturated aq. NH₄Cl followed by 3 N HCl and extraction with ethyl acetate. The organic layer was washed with brine, dried over Na₂SO₄ and the solvent was removed under reduced pressure to give a mixture of **8** and **9**, which was taken to next step without purification. ¹H NMR (CDCl₃, 200 MHz): δ 7.82–7.60 (m, 2H), 7.20–6.85 (m, 2H), 6.40–6.05 (m, 3H), 5.35–5.05 (m, 1H), 3.85 and 3.83 (s each, together 3H), 3.48 and 3.41 (s each, together 6H), 3.65–3.50 (m, 1H).

1-(4'-Methoxycarbonylphenyl)-2-(3'',5''-dimethoxyphenyl)propan-1,3-diol, 10a, 11a. A Solution of BH₃·SMe₂ (2M in THF, 10 mL) was added dropwise to a solution of the above-mentioned mixture of **8** and **9** and the reaction mixture was stirred overnight at room temperature. Solvents were removed under reduced pressure and the residue was purified by column chromatography (silica gel, hexanes–ethyl acetate) to afford a mixture of diols **10a** and **11a** (2.3 g, 66% for both steps). ¹H NMR (CDCl₃, 200 MHz): δ 7.91 and 7.80 (d, *J* = 8.2 Hz each, together 2H), 7.27 and 7.15 (d, *J* = 8.2 Hz each, together 2H), 6.35–6.05 (m, 3H), 5.04 and 4.96 (d each, *J* = 6.2 and 7.2 Hz, together 1H), 3.86 and 3.83 (s each, together 3H), 3.73 and 3.68 (s each, together 3H), 3.70 and 3.62 (s each, together 3H), 3.95–3.60 (m, 2H), 3.05 (m, 1H), 2.65 (br s, 2H).

2-(4'-Methoxycarbonylphenyl)-3-(3'',5''-dimethoxyphenyl)oxetane, 12, 13. TsCl (1.01 g, 5.3 mmol) was added to a solution of the mixture of **10a** and **11a** (1.53 g, 4.42 mmol) in dry pyridine (15 mL) at 0 °C. After stirring for 16 h, the mixture was worked up with water and CH₂Cl₂. The organic layer was washed with dilute HCl and with brine. Solvents were removed under reduced pressure and the residue was filtered through silica gel (hexanes–ethyl acetate) to afford a mixture of tosylates **10b** and **11b** (1.83 g, 83%).

A freshly prepared LDA solution in THF (4 mmol) was added dropwise to a solution of the mixture of **10b** and **11b** (1.83 g) in dry THF (20 mL) at 0 °C. The mixture was stirred at 60 °C for 0.5 h, then cooled to room temperature and worked up with saturated aq. NH₄Cl and ether. The combined organic layer was washed with brine, dried over Na₂SO₄ and solvent was removed under reduced pressure. The crude residue was separated over silica gel (hexanes–ethyl acetate) to afford compounds **12** and **13** separately. ¹H NMR of **12** (CDCl₃, 200 MHz): δ 7.85 (d, *J* = 8.0 Hz, 2H), 7.17 (d, *J* = 8.0 Hz, 2H), 6.20 (d, *J* = 8.6 Hz, 1H), 6.15 (d, *J* = 2.0 Hz, 2H), 6.14 (t, *J* = 2.0 Hz, 1H), 5.14 (dd, *J* = 8.6, 6.5 Hz, 1H), 4.84 (t, *J* = 6.6 Hz, 1H), 4.51 (q, *J* = 6.6 Hz, 1H), 3.84 (s, 3H), 3.58 (s, 6H). ¹H NMR of **13** (CDCl₃, 200 MHz): δ 8.05 (d, *J* = 8.3 Hz, 2H), 7.47 (d, *J* = 8.3 Hz, 2H), 6.52 (d, *J* = 2.0 Hz, 2H), 6.38 (t, *J* = 2.0 Hz, 1H), 5.78 (d, *J* = 6.9 Hz, 1H), 4.91 (m, 2H), 3.93 (m, 1H), 3.90 (s, 3H), 3.79 (s, 6H).

Structure Determination of Oxetanes 12 and 13. In Analogy to the reports on the isomeric diphenyloxetanes,⁴⁵ the cis isomer, **12**, has a lower *R_f* value compared with the trans isomer, **13**, on a silica gel plate with hexanes–ethyl acetate. Furthermore, the C-2 hydrogen in compound **13** appears at higher field (δ 5.78) in comparison with

compound **12** (δ 6.20). Moreover, in compound **12**, the C-2 hydrogen (at δ 6.20) exhibits NOE effect caused by the proximity of the C-3 hydrogen. No such effect is observed with isomer **13**.

2-(4'-Hydroxycarbonylphenyl)-3-(3'',5''-dimethoxyphenyl)oxetane, 6, 7. Compound **12** (60 mg) in methanol-THF (1:1, 4 mL) was treated with aq. NaOH (1 M, 2.5 mL) for 16 h. The reaction was cooled with an ice–water bath, diluted with ethyl acetate, acidified with aq. HCl (1N), and extracted with ethyl acetate. The combined organic layer was washed with brine, dried over Na₂SO₄ and the solvent was removed under reduced pressure. The crude residue was filtered over silica gel (hexanes–ethyl acetate) to afford compound **6** (45 mg). ¹H NMR (CDCl₃, 200 MHz): δ 7.92 (d, *J* = 8.0 Hz, 2H), 7.21 (d, *J* = 8.0 Hz, 2H), 6.23 (d, *J* = 8.5 Hz, 1H), 6.16 (s, 3H), 5.17 (t, *J* = 7.2 Hz, 1H), 4.86 (t, *J* = 6.3 Hz, 1H), 4.53 (q, *J* = 7.4 Hz, 1H), 3.59 (s, 6H).

In a similar manner, compound **13** (60 mg) was hydrolyzed to afford acid **7** (42 mg). ¹H NMR (CDCl₃, 200 MHz): δ 8.14 (d, *J* = 8.0 Hz, 2H), 7.52 (d, *J* = 8.0 Hz, 2H), 6.56 (d, *J* = 2.0 Hz, 2H), 6.40 (s, 1H), 5.85 (d, *J* = 6.9 Hz, 1H), 4.96 (m, 2H), 3.97 (m, 1H), 3.80 (s, 6H).

Ethyl 4-(3',5'-dimethoxyphenyl)butyrate, 15a.⁴⁶ An oven dried three-necked flask was loaded with Mg (2.82 g, 0.116 mol) and a small volume of dry THF. The Mg was activated by the addition of a few drops of dibromoethane. Solution of 5-chloro-1,3-dimethoxybenzene (**14a**, 10 g, 0.058 mol) in THF (20 mL) was added dropwise and the mixture was refluxed for 6 h. A mixture of ethyl 4-iodobutyrate (14 g, 0.058 mol) and Li₂CuCl₄ (0.1M in THF, 14.4 mL) was prepared under argon and cooled to 0 °C. The above-described Grignard solution was added via syringe over 30 min, the mixture was stirred at 0 °C for 30 min and then allowed to warm slowly to room-temperature overnight. The mixture was acidified with HCl (6M, 20 mL) and extracted with diethyl ether (3 × 30 mL). The organic layer was washed with 15% aq. NH₄OH (40 mL), water (30 mL) and brine (30 mL). The combined organic layer was dried over Na₂SO₄, solvents were removed under reduced pressure and the residue was purified over two consecutive silica gel columns. (hexane:ethyl acetate 9:1) followed by another column (benzene) to give compound **15a** in the form of a yellowish oil (4.16 g, 30%). ¹H NMR (200 MHz, CDCl₃): 6.32 (d, *J* = 1.9 Hz, 2H), 6.29 (t, *J* = 1.9 Hz, 1H), 4.11 (q, *J* = 7.1 Hz, 2H), 3.76 (s, 6H), 2.57 (t, *J* = 7.6 Hz, 2H), 2.30 (t, *J* = 7.4 Hz, 2H), 1.92 (quintet *J* = 7 Hz, 2H), 1.23 (t, *J* = 7.1 Hz, 3H); ¹³C NMR (200 MHz, CDCl₃): 173.5, 160.8, 143.8, 106.6, 98.0, 60.2, 55.2, 35.4, 33.6, 26.3, 14.2 ppm. MS (EI): 252 (M⁺).

4-(3',5'-Dimethoxyphenyl)butyraldehyde, 16a. DIBAL-H (1.5 M in toluene, 4.4 mL, 6.6 mmol) was added dropwise to a solution of **15a** (1.34 g, 5.32 mmol) in dry CH₂Cl₂ (20 mL) at –78 °C. After stirring for 1 h, the mixture was quenched with saturated aq. NH₄Cl (1.4 mL), diatomaceous earth (1 g) was added, the mixture was diluted with diethyl ether (10 mL) and the temperature was raised to 0 °C. After stirring for an additional 0.5 h, more diethyl ether was added, the mixture was dried over Na₂SO₄ and filtered, solvents were removed under reduced pressure and the residue was purified over silica gel (hexanes–ethyl acetate from 8:2 to 7:3) to give **16a** (777 mg, 70%) in the form of a colorless oil. ¹H NMR (200 MHz, CDCl₃): 9.73 (t, *J* = 1.6 Hz, 1H), 6.30 (s, 3H), 3.76 (s, 6H), 2.58 (t, *J* = 7.5 Hz, 2H), 2.44 (t, *J* = 7.6 Hz, 2H), 1.85–2.00 (quintet, *J* = 7.5 Hz, 2H). MS (CI): 209.1 (M⁺).

1-[4'-(Dioxolan-2"-yl)phenyl]-4-(3'',5''-dimethoxyphenyl)butan-1-ol, 17a. An oven dried three-necked flask was loaded with Mg (300 mg, 12.5 mmol). The surface of the Mg was covered with dry THF and was activated by few drops of dibromoethane. 1-(4'-Bromophenyl)-1,3-dioxolane (available from TCI America), was added dropwise and the progress of the reaction was followed by GC. The solution was warmed to 40 °C and stirred for 40 min, then cooled to room temperature. Aldehyde **16a** (527 mg, 2.53 mmol) was dissolved in THF (10 mL) and cooled to 0 °C. The Grignard reagent solution was slowly

(45) Fleming, S. A.; Gao, J. J. *Tetrahedron Lett.* **1997**, 38, 5407–5410.

(46) Kenny, M. J.; Mander, L. N.; Sethi, S. P. *Tetrahedron Lett.* **1986**, 27, 3923.

added via a syringe. The mixture was stirred at 0 °C for 15 min and then allowed to warm to room temperature and stirred for additional 30 min. The reaction was quenched with saturated aq. NH_4Cl and extracted with diethyl ether. The combined organic phase was washed with brine, dried over MgSO_4 . Solvents were removed under reduced pressure. The crude product was purified over silica gel (hexanes–ethyl acetate 8:2) to give **17a** (580 mg, 64%). ^1H NMR (200 MHz, CDCl_3): 7.43 (d, $J = 8.3$ Hz, 2H), 7.31 (d, $J = 8.3$ Hz, 2H), 6.30 (m, 3H) 5.78 (s, 1H), 4.67 (t, $J = 6.9$ Hz, 1H), 3.97–4.15 (m, 4H), 3.74 (s, 6H), 2.53 (t, $J = 7.2$ Hz, 2H), 1.56–1.89 (m, 4H).

1-[4'-(Dioxolan-2''-yl)phenyl]-4-(3''',5'''-dimethoxyphenyl)butan-1-one, 18a. PCC (1.99 g, 9.2 mmol) and diatomaceous earth (2 g) were added to a stirring solution of alcohol **17a** (1.65 g, 4.6 mmol) in CH_2Cl_2 (20 mL) at room temperature. After 1 h the brown mixture was filtered through silica gel and washed with ethyl acetate. The solvents were removed under reduced pressure and the crude product was purified by column chromatography (silica gel, hexanes–ethyl acetate 7:3) to give **18a** (1.17 g, 72%). ^1H NMR (200 MHz, CDCl_3): 7.91 (d, $J = 8.2$ Hz, 2H), 7.53 (d, $J = 8.2$ Hz, 2H), 6.33 (d, $J = 2.2$ Hz, 2H), 6.29 (t, $J = 2.2$ Hz, 1H), 5.78 (s, 1H) 4.02–4.11 (m, 4H), 3.75 (s, 6H), 2.95 (t, $J = 7.2$ Hz, 2H), 2.64 (t, $J = 7.5$ Hz, 2H), 2.05 (quintet, $J = 7.3$ Hz, 2H). MS (CI): 357.2 (MH^+).

1-(4'-Formylphenyl)-4-(3''',5'''-dimethoxyphenyl)butan-1-one, 19a. Compound **18a** (248 mg, 0.7 mmol) was dissolved in THF (5 mL) and H_2O (0.5 mL). PTSA (50 mg) was added and the mixture was stirred overnight. Saturated aq. NaHCO_3 was added and the mixture was extracted with diethyl ether. The combined organic phase was washed with brine, dried over MgSO_4 and solvents were removed under reduced pressure. The crude product was purified by column chromatography (silica gel, hexanes–ethyl acetate 7:3) to give **19a** (180 mg, 78.4%) in the form of a white solid. ^1H NMR (200 MHz, CDCl_3): 10.07 (s, 1H), 8.03 (d, $J = 8.2$ Hz, 2H), 7.93 (d, $J = 8.2$ Hz, 2H), 6.33 (d, $J = 1.7$ Hz, 2H), 6.30 (t, $J = 1.7$ Hz, 1H), 3.75 (s, 6H), 2.99 (t, $J = 7.1$ Hz, 2H), 2.66 (t, $J = 7.4$ Hz, 2H), 2.07 (quintet, $J = 7.3$, 2H). MS (CI): 313.2 (MH^+).

1-(4'-Hydroxycarbonylphenyl)-4-(3''',5'''-dimethoxyphenyl)butan-1-one, 1a. A solution of **19a** (97 mg, 0.31 mmol) in *t*-BuOH (2.3 mL) was diluted with aq. potassium phosphate buffer (1.25 M pH 4, 1.5 mL). Aqueous KMnO_4 (1 M, 2.3 mL) was added with vigorous stirring, the mixture was stirred at room temperature for 10 min and then quenched by the addition of saturated aq. Na_2SO_3 . The resultant pH of the mixture was adjusted to 3 with dilute HCl, and extracted with diethyl ether. The combined organic phase was washed with brine, dried over MgSO_4 and solvents were removed under reduced pressure. The crude product was purified by column chromatography (silica gel, hexanes–ethyl acetate 7:3 + 0.5% acetic acid) to give **1** (52 mg, 51%) in the form of a white solid. ^1H NMR (200 MHz, CDCl_3): 8.15 (d, $J = 8.3$ Hz, 2H), 7.96 (d, $J = 8.3$ Hz, 2H), 6.33 (br s, 2H), 6.30 (br s, 1H), 3.75 (s, 6H), 3.99 (t, $J = 7.1$ Hz, 2H), 2.66 (t, $J = 7.4$ Hz, 2H), 2.09 (quintet, $J = 7.1$ Hz, 2H). MS (CI): 328 (M^-).

Physical Data of Similarly Prepared Analogues:

Ethyl 4-(3'-methoxyphenyl)butyrate, 15b.⁴⁷ This analogue was prepared from 3-methoxy-1-bromobenzene. ^1H NMR (200 MHz, CDCl_3): 7.22–7.14 (m, 1H), 6.77–6.71 (m, 3H), 4.10 (q, $J = 7.4$ Hz, 2H), 3.78 (s, 3H), 2.61 (t, $J = 7.3$ Hz, 2H), 2.28 (t, $J = 7.3$ Hz, 2H), 1.97 (quintet, $J = 7.3$ Hz, 2H), 1.23 (t, $J = 7.4$ Hz, 3H). MS (CI): 223.2 (MH^+).

4-(3'-Methoxyphenyl)butyraldehyde, 16b.⁴⁸ ^1H NMR (200 MHz, CDCl_3): 9.74 (br s, 1H), 7.19 (br t, $J = 7.8$ Hz, 1H), 6.70 (m, 3H), 3.78 (s, 3H), 2.62 (t, $J = 7.4$ Hz, 2H), 2.44 (t, $J = 7.7$ Hz, 2H), 1.94 (quintet, $J = 7.5$ Hz, 2H). MS (CI): 179.1 (MH^+).

1-[4'-(Dioxolan-2''-yl)phenyl]-4-(3'''-methoxyphenyl)butan-1-ol, 17b. ^1H NMR (200 MHz, CDCl_3): 7.43 (d, $J = 8.2$ Hz, 2H), 7.31 (d, $J = 8.2$ Hz, 2H), 6.73–6.68 (m, 4H), 5.78 (s, 1H), 4.67 (t, $J = 6.9$ Hz, 1H), 4.15–4.00 (m, 4H), 3.76 (s, 3H), 2.57 (t, $J = 7.3$ Hz, 2H), 1.88–1.75 (m, 4H). MS (CI): 329.0 (MH^+).

1-[4'-(Dioxolan-2''-yl)phenyl]-4-(3'''-methoxyphenyl)butan-1-one, 18b. ^1H NMR (200 MHz, CDCl_3): 7.91 (d, $J = 8.2$ Hz, 2H), 7.53 (d, $J = 8.2$ Hz, 2H), 7.18 (t, $J = 8.2$ Hz, 1H), 6.79–6.71 (m, 3H), 5.83 (s, 1H), 4.17–4.02 (m, 4H), 3.77 (s, 3H), 2.96 (t, $J = 7.2$ Hz, 2H), 2.68 (t, $J = 7.3$ Hz, 2H), 2.03 (quintet, $J = 7.3$ Hz, 2H). MS (CI): 327.0 (MH^+).

1-(4'-Formylphenyl)-4-(3''-methoxyphenyl)butan-1-one, 19b. ^1H NMR (200 MHz, CDCl_3): 10.08 (s, 1H), 8.03 (d, $J = 8.3$ Hz, 2H), 7.93 (d, $J = 8.3$ Hz, 2H), 7.21–7.13 (m, 1H), 6.79–6.68 (m, 3H), 3.77 (s, 3H), 2.99 (t, $J = 7.1$ Hz, 2H), 2.70 (t, $J = 7.1$ Hz, 2H), 2.08 (quintet, $J = 7.1$ Hz, 2H). MS (CI): 283.1 (MH^+).

1-(4'-Hydroxycarbonylphenyl)-4-(3''-methoxyphenyl)butan-1-one, 1b. ^1H NMR (200 MHz, CDCl_3): 8.15 (d, $J = 8.4$ Hz, 2H), 7.97 (d, $J = 8.4$ Hz, 2H), 7.17 (m, 1H), 6.79–6.69 (m, 3H), 3.77 (s, 3H), 3.00 (t, $J = 7.2$ Hz, 2H), 2.72 (t, $J = 7.2$ Hz, 2H), 2.08 (quintet, $J = 7.2$ Hz, 2H). MS (CI): 299.1 (MH^+).

Ethyl 4-Phenylbutyrate, 15c. (prepared by the esterification of 4-Phenyl-butyric acid) ^1H NMR (200 MHz, CDCl_3): 7.31–7.14 (m, 5H), 3.65 (s, 3H), 2.64 (t, $J = 7.4$ Hz, 2H), 2.32 (t, $J = 7.3$ Hz, 2H), 1.94 (quintet, $J = 7.4$ Hz, 2H). MS (CI): 179.0 (MH^+). MS (CI): 179.0 (MH^+).

4-Phenylbutyraldehyde, 16c.⁴⁹ ^1H NMR (200 MHz, CDCl_3): 9.74 (t, $J = 1.5$ Hz, 1H), 7.32–7.14 (m, 5H), 2.65 (t, $J = 7.3$ Hz, 2H), 2.44 (td, $J = 7.7$ Hz, 1.4 Hz, 2H), 1.95 (quintet, $J = 7.7$ Hz, 2H). MS (CI): 149 (MH^+).

1-[4'-(Dioxolan-2''-yl)phenyl]-4-phenylbutan-1-ol, 17c. ^1H NMR (200 MHz, CDCl_3): 7.45 (d, $J = 8.2$ Hz, 2H), 7.33 (d, $J = 8.2$ Hz, 2H), 7.26–7.12 (m, 5H), 5.80 (s, 1H), 4.70 (t, $J = 6.9$ Hz, 1H), 4.14–4.02 (m, 4H), 2.62 (t, $J = 7.2$ Hz, 2H), 1.79–1.63 (m, 4H). MS (CI): 299.2 (MH^+).

1-[4'-(Dioxolan-2''-yl)phenyl]-4-phenylbutan-1-one, 18c. ^1H NMR (200 MHz, CDCl_3): 7.90 (d, $J = 8.3$ Hz, 2H), 7.53 (d, $J = 8.3$ Hz, 2H), 7.32–7.16 (m, 5H), 5.83 (s, 1H), 4.15–3.99 (m, 4H), 2.95 (t, $J = 7.1$ Hz, 2H), 2.70 (t, $J = 7.5$ Hz, 2H), 2.06 (quintet, $J = 7.1$ –7.5 Hz, 2H). MS (CI): 297.1 (MH^+).

1-(4'-Formylphenyl)-4-phenylbutan-1-one, 19c. ^1H NMR (200 MHz, CDCl_3): 10.08 (s, 1H), 8.03 (d, $J = 8.2$ Hz, 2H), 7.93 (d, $J = 8.2$ Hz, 2H), 7.33–7.15 (m, 5H), 2.99 (t, $J = 7.2$, 2H), 2.72 (t, $J = 7.5$ Hz, 2H), 2.08 (quintet, $J = 7.4$ Hz, 2H). MS (CI): 253.1 (MH^+).

1-(4'-Hydroxycarbonylphenyl)-4-phenylbutan-1-one, 1c. ^1H NMR (200 MHz, CDCl_3): 8.17 (d, $J = 8.3$ Hz, 2H), 7.96 (d, $J = 8.3$ Hz, 2H), 7.33–7.16 (m, 5H), 2.99 (t, $J = 7.1$ Hz, 2H), 2.72 (t, $J = 7.1$ Hz, 2H), 2.08 (quintet, $J = 7.1$ Hz, 2H). MS (CI): 269.1 (MH^+).

Irradiation of 18a. Ketone **18a** (676 mg, 1.98 mmol) was dissolved in acetone (10 mL) under argon, the solution was flushed with argon for 10 min and then irradiated with a mercury lamp for 7 h. The solvent was removed under reduced pressure and the residue was separated by flash column chromatography (silica gel, 2–10% ethyl acetate in benzene) to give **2** (127 mg, 41%), **20** (165 mg, 45.5%), **21** (33 mg, 4.9%), and **22** (35 mg, 5.2%).

3,5-Dimethoxystyrene, 2. ^1H NMR (200 MHz, CDCl_3): 6.61–6.70 (dd, $J = 17.4$, 10.8 Hz, 1H), 6.55 (d, $J = 2.2$ Hz, 2H), 6.37 (t, $J = 2.2$ Hz, 1H), 5.71 (d, $J = 17.4$ Hz, 1H), 5.23 (d, $J = 10.8$ Hz, 1H), 3.79 (s, 6H). MS (CI): 165.0 (MH^+).

4-(Dioxolan-2-yl)acetophenone, 20. ^1H NMR (200 MHz, CDCl_3): 7.95 (d, $J = 8.2$ Hz, 2H), 7.55 (d, $J = 8.2$ Hz, 2H), 5.85 (s, 1H), 3.00–4.14 (m, 4H), 2.59 (s, 3H). MS (CI): 193.2 (MH^+).

cis-1-[4'-(Dioxolan-2''-yl)phenyl]-2-(3''',5'''-dimethoxyphenyl)cyclobutan-1-ol, 21. ^1H NMR (200 MHz, CDCl_3): 7.30 (d, $J = 8.3$ Hz,

(47) Oikawa, Y.; Kurosawa, T.; Yonemitsu, O. *Chem. Pharm. Bull.* **1975**, 23, 2466.

(48) Nagumo, S.; Miyoshi, I.; Akita, H.; Kawahara, N. *Tetrahedron Lett.* **2002**, 43, 2223–2226.

(49) Zelechonok, Y.; Silverman, R. B. *J. Org. Chem.* **1992**, 57, 5785–5787.

2H), 7.24 (d, $J = 8.3$ Hz, 2H), 6.12 (t, $J = 2.2$ Hz, 1H), 5.96 (d, $J = 2.2$ Hz, 2H), 5.72 (s, 1H), 3.96–4.09 (m, 4H), 3.79 (dd, $J = 10.3, 9.2$, Hz, 1H), 3.57 (s, 6H), 2.70–2.78 (m, 1H), 1.86–2.41 (m, 3H). MS (EI): 356 (M^+).

trans-1-[4'-(Dioxolan-2''-yl)phenyl]-2-(3'',5''-dimethoxyphenyl)-cyclobutan-1-ol, 22. ^1H NMR (200 MHz, CDCl_3): 7.52 (d, $J = 8.7$ Hz, 2H), 7.46 (d, $J = 8.7$ Hz, 2H), 6.33 (d, $J = 1.9$ Hz, 2H), 6.30 (t, $J = 1.9$ Hz, 1H), 5.80 (s, 1H), 3.98–4.15 (m, 4H), 3.90 (t, $J = 8.0$ Hz, 1H), 3.72 (s, 6H), 2.43–2.54 (m, 2H), 2.17–2.30 (m, 2H). MS (EI): 356 (M^+).

Determination of Stereochemistry of the cis- and trans-Cyclobutan Derivatives. A literature report on the structure of cis- and trans-1,2-diphenylcyclobutanols was unequivocally supported by X-ray crystallography of the cis isomer.²² The reported ^1H NMR data of these isomers differ significantly from one another, particularly in the region of 1.8–3.0 ppm, which represents the cyclobutanol methylene. Since the NMR spectra of our isomers, 21 and 22 matched the reported spectra of 1,2-diphenylcyclobutanols, the relative stereochemistry of our compounds was also determined unequivocally. This assignment was further confirmed by NOE experiments. Significant NOE effect was observed with the trans isomer, 22. We carried out a 1D NOE experiment and used multiple selective frequency version of NOE, where each line of a multiplet was irradiated for a short period of time within a narrow bandwidth. The NOE experiment confirmed the assignment of the trans isomer (data not shown) with its benzylic hydrogen at 3.9 ppm exhibiting proximity to both aromatic rings, a situation that was not seen with the cis isomer. Our assumption that the less polar cyclobutanol (as seen on a TLC plate) was the trans isomer was thus confirmed by NMR spectroscopy.

cis-1-[4'-Formylphenyl]-2-(3'',5''-dimethoxyphenyl)cyclobutan-1-ol, 23. Compound 21 (13 mg, 0.037 mmol) was dissolved in THF (9 mL) and H_2O (1 mL). PTSA (10 mg) was added and the mixture was stirred overnight. A solution of saturated aq. NaHCO_3 was added and the mixture was extracted with diethyl ether. The combined organic phase was washed with brine, dried over MgSO_4 , and solvents were removed under reduced pressure. The crude product was purified by flash column chromatography (silica gel, hexanes–ethyl acetate 3:7) to give 23 (7 mg, 61.5%). ^1H NMR (200 MHz, CDCl_3): 9.90 (s, 1H), 7.68 (d, $J = 8.3$ Hz, 2H), 7.43 (d, $J = 8.3$ Hz, 2H), 6.11 (t, $J = 2.2$ Hz, 1H), 5.98 (d, $J = 2.2$ Hz, 2H), 3.86 (t, $J = 9.8$ Hz, 1H), 3.58 (s, 6H), 2.79 (br t, $J = 9.8$ Hz, 1H), 1.97–2.43 (m, 3H). MS (CI): 313.2 (M^+).

trans-1-[4'-Formylphenyl]-2-(3'',5''-dimethoxyphenyl)cyclobutan-1-ol, 24. The synthesis of 24 from 22 was analogous to that of 23 from 21. The crude product was purified by flash column chromatography (silica gel, hexanes–ethyl acetate 2:8) to give 24 (24 mg, 77%). ^1H NMR (200 MHz, CDCl_3): 9.99 (s, 1H), 7.67 (d, $J = 8.2$ Hz, 2H), 7.66 (d, $J = 8.2$ Hz, 2H), 6.34 (t, $J = 2.2$ Hz, 1H), 6.25 (d, $J = 2.1$ Hz, 2H), 3.93 (t, $J = 8.1$ Hz, 1H), 3.72 (s, 6H), 2.55–2.66 (m, 2H), 2.26–2.35 (m, 2H). MS (CI): 313.2 (M^+).

cis-1-[4'-Hydroxycarbonylphenyl]-2-(3'',5''-dimethoxyphenyl)cyclobutan-1-ol, 4. A solution of 23 (18 mg, 0.058 mmol) in $t\text{-BuOH}$ (0.6 mL) was diluted with aq. potassium phosphate buffer (1.25 M, pH = 4, 0.3 mL) and treated with aq. KMnO_4 (1 M, 0.53 mL) at room temperature as described above for the conversion of 19a to 1a. Compound 4 was obtained (18.9 mg, 100%) in the form of a white solid. ^1H NMR (200 MHz, CD_3OD): 7.79 (d, $J = 8.2$ Hz, 2H), 7.38

(d, $J = 8.2$ Hz, 2H), 6.10 (t, $J = 2.2$ Hz, 1H), 5.99 (d, $J = 2.2$ Hz, 2H), 3.83 (t, $J = 9.8$ Hz, 1H), 3.56 (s, 6H), 2.76 (br t, $J = 9.8$ Hz, 1H), 1.97–2.43 (m, 3H).

trans-1-[4'-Hydroxycarbonylphenyl]-2-(3'',5''-dimethoxyphenyl)-cyclobutan-1-ol, 5. The synthesis followed the same procedure as for compound 4. The crude product was purified by column chromatography (silica gel, hexanes–ethyl acetate 1:1) to give 5 (13.6 mg, 98%). ^1H NMR (200 MHz, CDCl_3): 8.10 (d, $J = 8.4$ Hz, 2H), 7.61 (d, $J = 8.4$ Hz, 2H), 6.35 (t, $J = 2.1$ Hz, 1H), 6.27 (d, $J = 2.1$, 2H), 3.93 (t, $J = 8.4$ Hz, 1H), 3.73 (s, 6H), 2.48–2.67 (m, 2H), 2.21–2.34 (m, 2H).

Wavelength Dependence Experiments. An Oriel Xe 300–1000W lamp model 6269 was used as the light source. An Acton Research Corporation Spectra Pro – 275 monochromator with 0.275 m triple grating was used. Light intensities were measured using an Ophir Nova laser star energy monitor with a p-type thermophile absorber head. A scale of relative intensities was constructed and sample was irradiated at each wavelength for the appropriate time, so that all samples would receive the same amount of irradiation and all results would remain at less than 20% conversion. The samples were placed at the monochromator light exit using Starna quartz cuvettes with 1 mm cell length. Each sample consisted of 50 μL solution. Experiments with Antibodies were performed with equal concentration of antibody and substrate, 50 μM in PBS (pH 7.4) and 10% CH_3CN . Background experiments were performed using the same conditions, omitting the antibody. All solutions were stored at 0 $^\circ\text{C}$. Each sample was thawed and injected to HPLC. No change in results was observed whether the sample was injected immediately after irradiation or 2 days later. All experiments were carried out in duplicates.

Nucleotide Sequencing of Antibody 20F10. Total mRNA was obtained from 5×10^6 hybridoma cells using Rneasy Midi Kit (Qiagen #75142). The cDNA was prepared from 2 μg of total RNA with First Strand cDNA Synthesis Kit for RT-PCR (Roche #1488 188). After amplification by polymerase chain reaction the light and heavy chains were cloned separately into pCR4-TOPO using TOPO TA Cloning Kit for Sequencing (Invitrogen K4575–01).⁵⁰

The primers used for the light chain were as follows:

3'-GAYATHGTNATGACNCAR (forward) and

3'-GCGCCGTCTAGAATTAACACTCATTCCTGTTGAA (reverse)

The primers used for the heavy chain were:

3'-GCCAGCCGCCATGGCA (forward)

3'-TATGCAACTAGTACAACCACAATCCCTGGG (reverse)

Clones, which contained the correct size insert (approximately 330 base pairs), were sequenced and analyzed using the Blast program.

Acknowledgment. E. K. thanks the Israel-US Binational Science Foundation, the German-Israeli Project Cooperation (DIP), and the Skaggs Institute for Chemical Biology. K. N. H. thanks the National Science Foundation and the National Institute of General Medical Sciences, National Institutes of Health. Y. Hu thanks UCLA Academic Technology Services (ATS) for providing computation time. We thank Diane Kubitz and Terri Jones of TSRI for the sequencing of antibody 20F10.

JA045419U

(50) TOPO TA Cloning kit for sequencing, Instruction Manual, version J, Invitrogen life sciences, pp 4–8.